AD-A065 620 ARMY MILITARY PERSONNEL CENTER ALEXANDRIA VA F/G 9/1
THE THREE STUB ALIGNMENT METHOD FOR MAXIMIZING TRANSMISSION THR--ETC(U)
AUG 78 D F RICHARDS

UNCLASSIFIED NL

1 OF 1
AD
A065820

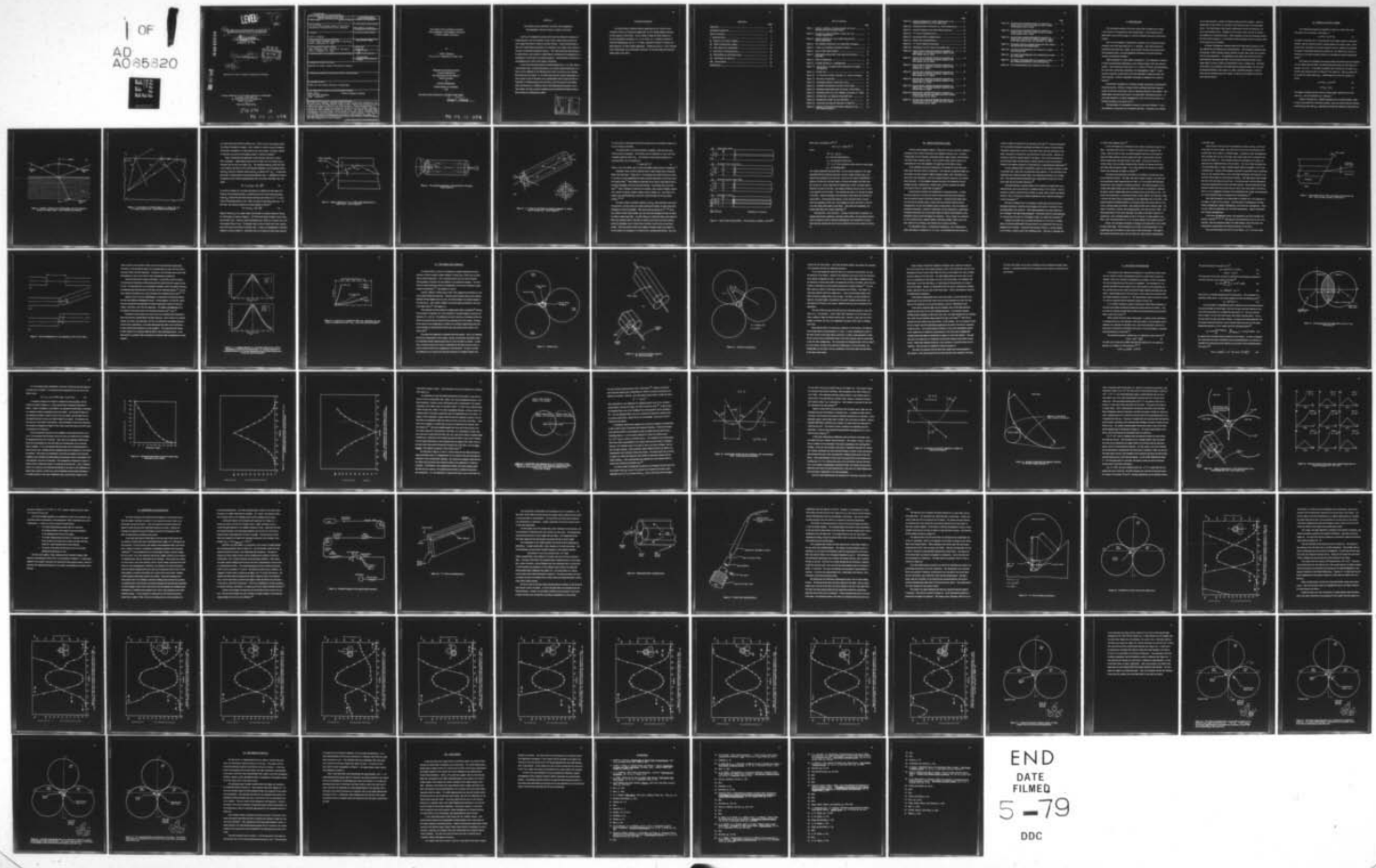

END
DATE FILMED
5-79
DDC

(2)

(6) THE THREE STUB ALIGNMENT METHOD FOR MAXIMIZING TRANSMISSION THROUGH OPTICAL FIBER JUNCTIONS.

(10) CPT DAVID F. RICHARDS
HQDA, MILPERCEN (DAPC-OPP-E)
200 Stoval Street
Alexandria, VA 22332

(9) Final Report, (11) 29 Aug 78

(12) 92p.

Approved for public release; distribution unlimited

A thesis submitted to the Florida Institute of Technology
in partial fulfillment of
the requirements for the degree of
Master of Science
in
Electrical Engineering

391 191 LB

UNCLASSIFIED

SECURITY CLASSIFICATION OF THIS PAGE *(When Data Entered)*

REPORT DOCUMENTATION PAGE		READ INSTRUCTIONS BEFORE COMPLETING FORM
1. REPORT NUMBER	2. GOVT ACCESSION NO.	3. RECIPIENT'S CATALOG NUMBER
4. TITLE *(and Subtitle)* The Three Stub Alignment Method for Maximizing Transmission Through Optical Fiber Junctions		5. TYPE OF REPORT & PERIOD COVERED Final Report, 29 Aug 78 6. PERFORMING ORG. REPORT NUMBER
7. AUTHOR(s) David F. Richards		8. CONTRACT OR GRANT NUMBER(s)
9. PERFORMING ORGANIZATION NAME AND ADDRESS Student, HQDA, MILPERCEN (DAPC-OPP-E), 200 Stoval Street, Alexandria, VA 22332		10. PROGRAM ELEMENT, PROJECT, TASK AREA & WORK UNIT NUMBERS
11. CONTROLLING OFFICE NAME AND ADDRESS HQDA, MILPERCEN, ATTN: DAPC-OPP-E, 200 Stoval Street, Alexandria, VA 22332		12. REPORT DATE 29 Aug 78 13. NUMBER OF PAGES 98
14. MONITORING AGENCY NAME & ADDRESS*(if different from Controlling Office)*		15. SECURITY CLASS. *(of this report)* UNCLASSIFIED 15a. DECLASSIFICATION/DOWNGRADING SCHEDULE

16. DISTRIBUTION STATEMENT *(of this Report)*

Approved for public release distribution unlimited

17. DISTRIBUTION STATEMENT *(of the abstract entered in Block 20, if different from Report)*

18. SUPPLEMENTARY NOTES

Thesis for the Florida Institute of Technology

19. KEY WORDS *(Continue on reverse side if necessary and identify by block number)*

Fiber optics
Optical-fiber waveguide
Fiber connectors
Optical waveguide coupling

20. ABSTRACT *(Continue on reverse side if necessary and identify by block number)*

The three rod alignment technique which has been utilized for splicing and connecting fibers, has been adapted to make a fiber coupler which produces an error signal when there is offset in the fiber junction. Proper interpretation of this error signal allows the junction to be adjusted to zero offset, thus maximizing the power transmitted through the junction. This thesis discusses light propagation in optical fibers, the structure of optical fibers, distributed and misalignment loss mechanisms, and the three rod coupler geometry. Both analytical and experimental investigations were made of the coupler's operation.

DD FORM 1 JAN 73 1473 EDITION OF 1 NOV 65 IS OBSOLETE

SECURITY CLASSIFICATION OF THIS PAGE *(When Data Entered)*

THE THREE STUB ALIGNMENT METHOD FOR MAXIMIZING TRANSMISSION THROUGH OPTICAL FIBER JUNCTIONS

by

David F. Richards
B.S. in E.E., University of Toledo, 1970

Submitted to the Graduate Faculty
in partial fulfillment of
the requirements for the degree of
Master of Science
in
Electrical Engineering
Florida Institute of Technology
1978

David F Richards

ABSTRACT

THE THREE STUB ALIGNMENT METHOD FOR MAXIMIZING TRANSMISSION THROUGH OPTICAL FIBER JUNCTIONS

The three rod alignment technique which has been utilized for splicing and connecting fibers, has been adapted to make a fiber coupler which produces an error signal when there is offset in the fiber junction. Proper interpretation of this error signal allows the junction to be adjusted to zero offset, thus maximizing the power transmitted through the junction. This thesis discusses light propagation in optical fibers, the structure of optical fibers, distributed and misalignment loss mechanisms, and the three rod coupler geometry. Both analytical and experimental investigations were made of the coupler's operation.

It was shown both theoretically and experimentally that 1) for offset displacements greater than a critical displacement, the relative offset displacement of the fibers can be identified by the differing power levels of the three error sensing fibers built into the coupler, 2) for offsets less than the critical displacement, the power levels in each of the three error sensing fibers will be equal and will vary identically for displacements in any direction, and 3) the power in the sensing fibers all decrease to a minimum value as the displacement decreases to zero. This coupler can then be used to maximize power transmitted through an optical fiber junction by minimizing the offset.

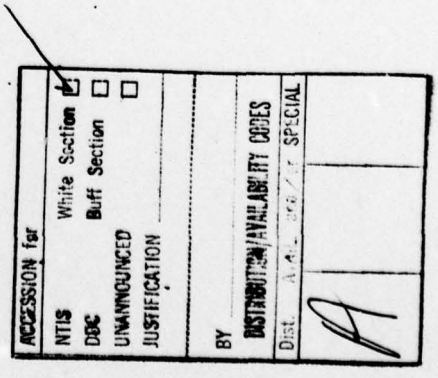

ACKNOWLEDGEMENT

The author wishes to express sincere appreciation to Dr. Marvin Drake, Assistant Professor of Electrical Engineering, for his valuable guidance throughout the progress of this thesis. He also wishes to thank the other members of the oral examination committee, Dr. A. W. Revay, Jr., Professor and Head of Electrical Engineering, and Dr. J. H. Blatt, Associate Professor of Physics and Space Sciences, for their helpful suggestions. Thanks also go to Dr. Larry Dworkin, of the United States Army Electronics Command, for his encouragement during the initial stages of the work.

CONTENTS

LIST OF FIGURES

Page

I. INTRODUCTION

The successful production of low loss optical fiber waveguides has opened a new frontier for development in telecommunications. It has transformed the optical fiber from medical useage to a vital and profitable electronic transmission medium.

Some of the advantages of optical fiber waveguide over conventional metalic conductors were best enumerated by M. K. Barnoski. They include increased bandwidths; decreased size, weight, and crosstalk; immunity from ground loops, electromagnetic pulse, and electromagnetic interference; increased intercept security; and dielectric isolation.[1]

Light propagates in a large range of frequencies. The frequencies of interest to optical communication applications are the visible and part of the near infrared regions. These frequencies range from 2 to 7.5 times 10^{14} hertz, and theoretically, this would allow information bandwidths in the high gigahertz range.[2] Present material properties of optical fibers limit the bandwidth to values far below this initial estimate. However, bandwidths of hundreds of megahertz are readily attainable.[3]

Optical fiber waveguides are currently carrying commercial communications with great success. However, because of their relatively small sizes (approximately 125 microns in diameter), they are extremely delicate to join together. Misaligned fibers can cause great losses in an optical fiber transmission system. At such small diameters, an offset misalignment of only a few microns means a noticeable percentage of the signal is lost.[4]

The fabrication of a demountable connector is even more difficult. It must join the fibers at extremely close tolerances each time. Connectors are available

for the large diameter, medium and high loss fibers and fiber bundles. However, applications for these fibers are limited to short distances due to the large signal losses. The long distance, high capacity applications lie with the multimode, low loss, small diameter fiber. Connectors for this type of fiber are only now becoming available on a commercial basis. Many companies are actively pursuing research into this area but because of the extremely lucrative potential of such a product, much of the results are not available.

The three rod alignment technique which will be described in section IV, has been utilized for both splicing and connecting fibers. This technique capitalizes upon the geometry of three mutually tangent cylinders of equal radii, which form an interstice of exact proportions. The application to this thesis was to hold the end of a small diameter communications fiber in the interstice between the ends of three larger fibers, all four of which are butted flush to form a coupler face. The object of this study is to investigate, both analytically and experimentally, the error signal gathering abilities of this coupler at a fiber connection interface. It will be shown that by minimizing the error signal, the fibers can be aligned so that their ends coincide exactly.

II. THEORY OF OPTICAL FIBERS

The concepts governing the propagation of light in an optical fiber start with Snell's law of refraction, (See Figure 1):

$$n_1 \sin \phi_1 = n_2 \sin \phi_2. \quad (1)$$

The index of refraction (n) is a measurement of the relative density of the optical medium, with the refractive index of vacuum defined to be equal to unity. In the present case, the index of air is also assumed to be one. Equation (1) describes the angular relationships between the incident ray, the reflected ray, and the refracted ray at an abrupt boundary between two homogeneous optical transmission media.[5]

When light rays traveling in one optical medium fall incident upon the boundary of a less dense optical medium, an optical phenomenon known as total internal reflection, can occur. As the angle of incidence (ϕ_1) is increased, the angle of refraction (ϕ_2) increases until it reaches 90° (see Figure 2). When ϕ_2 equals 90°, ϕ_1 equals the critical angle (ϕ_{1c}). Substituting these values into equation (1) yields:

$$n_1 \sin \phi_{1c} = n_2 \sin 90^\circ \quad (2)$$

$$\sin \phi_{1c} = n_2/n_1 \quad (3)$$

For angles of incidence greater than the critical angle, refracted rays do not exist (i.e., all of the incident ray is reflected).[7]

If light is launched into a cylinder fashioned from an optical medium, which in turn is surrounded by a less dense medium, those rays incident upon the cylinder wall with ϕ_1 greater than ϕ_{1c}, experience total internal reflection at that point and

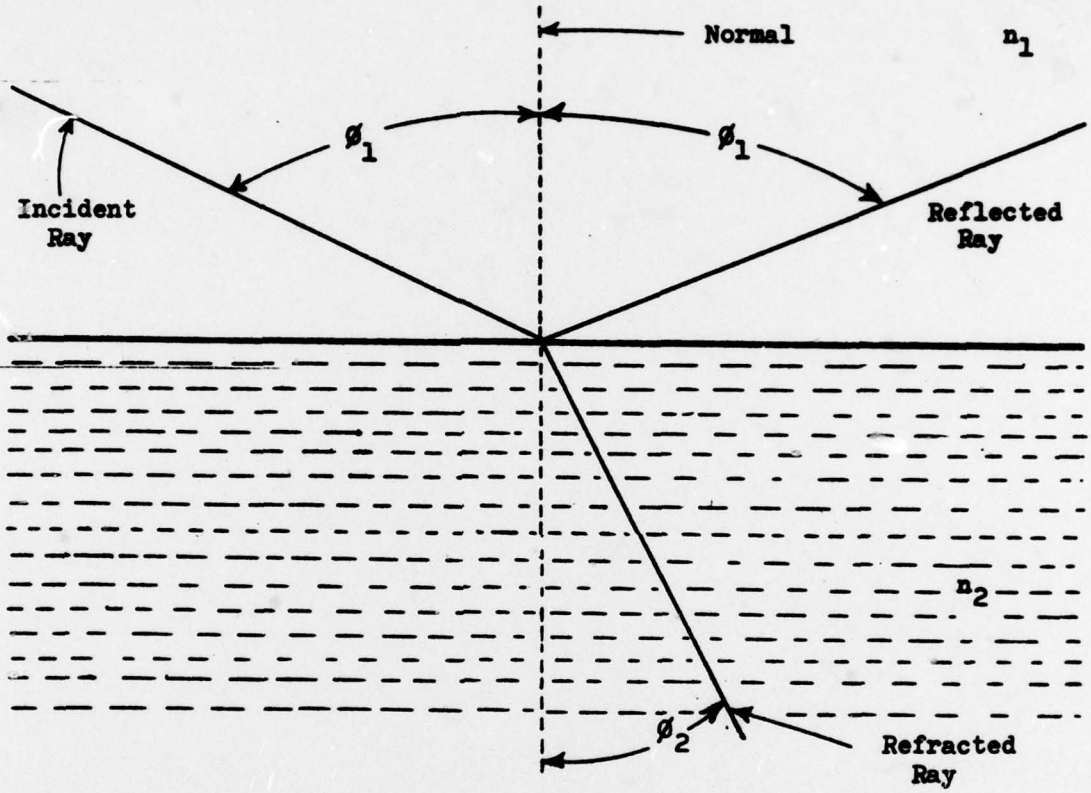

Figure 1. Incident, reflected, and refracted light rays at the interface between two optical media. (From Halliday and Resnick)[6]

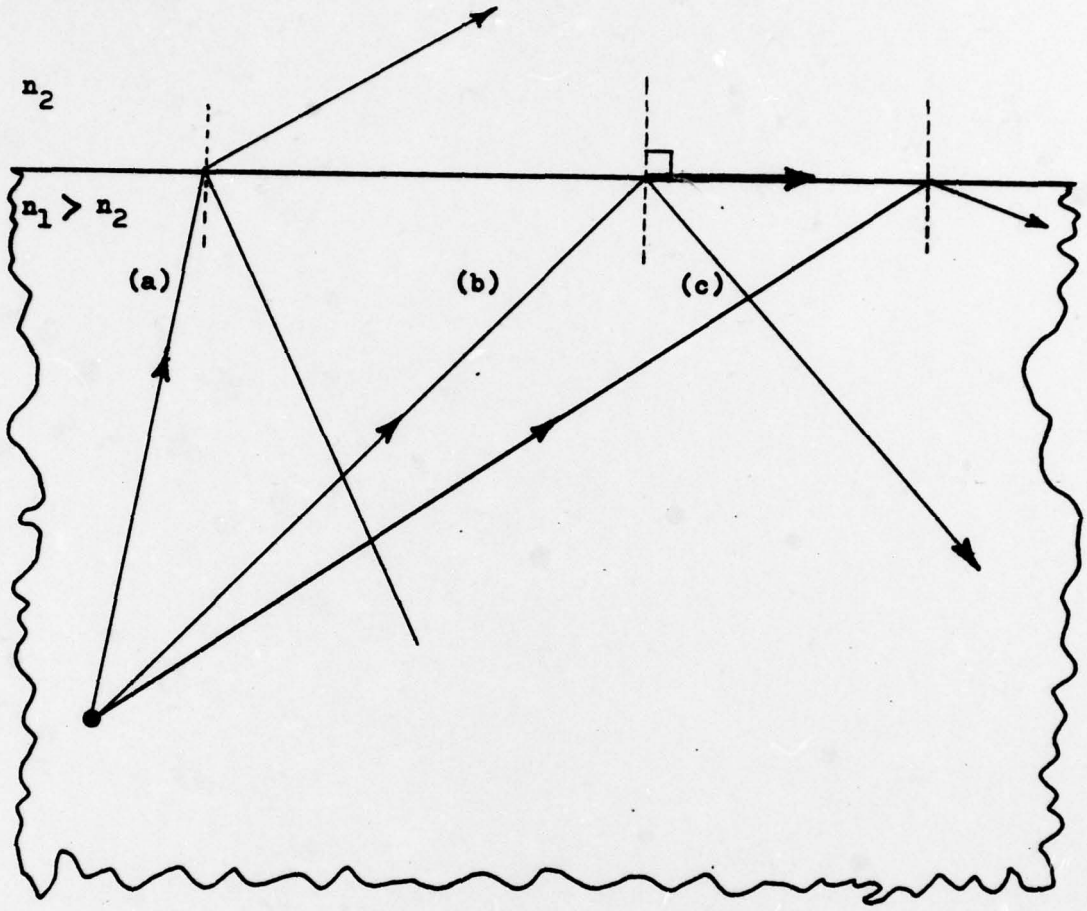

Figure 2. a) Ray prior to critical incidence, b) critical ray, and c) a totally reflected ray. (From Halliday and Resnick)[9]

any other intersection with the cylinder wall. Those rays are then trapped inside the cylinder throughout its length. Such a cylinder is called an optical waveguide. Optical fiber waveguides are constructed in this same manner, the inside cylinder is called the core and the surrounding medium is called the cladding.[8]

Figure 3 illustrates the application of total internal reflection to optical fiber waveguides. Light incident upon the end of a fiber core at an angle of Θ_o is refracted into the core at an angle of Θ_1. The maximum angle Θ_o which will yield a ray trapped in the fiber core by total internal reflection, is the launching critical angle Θ_{oc} where its refracted counter part Θ_{1c} is equal to $90^o - \phi_{1c}$. An important parameter of optical fibers is the numerical aperture (NA). A definition for numerical aperture can be found by applying Snell's law to the face of the fiber core, and yields:

$$NA = n_o \sin \Theta_{oc} = (n_1^2 - n_2^2)^{\frac{1}{2}} . \qquad (4)$$

As shown in equation (3), the numerical aperture is defined to be the index of refraction of the launching medium, multiplied by the sine of the largest launching angle (Θ_{oc}) which will yield total internal refraction in the fiber core.[11] In most cases the launching medium is air, where the index of refraction equals one. For this case, the numerical aperture is usually defined as follows:[12]

$$NA = \sin \Theta_{oc} = (n_1^2 - n_2^2)^{\frac{1}{2}} \qquad (5)$$

Figure 3 shows Θ_o to be a planar angle, but the fiber is actually cylindrical and Θ_o is a solid angle, as shown in Figure 4. All of the rays shown in Figure 3 and 4 intersect the fiber axis. These are called meridional rays, which are a special case to the more general class of rays. The general class of rays is called skew rays, because rays of this class travel skew to the fiber axis. A skew ray propagating in a dielectric cylinder is shown in Figure 5. Meridonal rays are of interest because their behavior

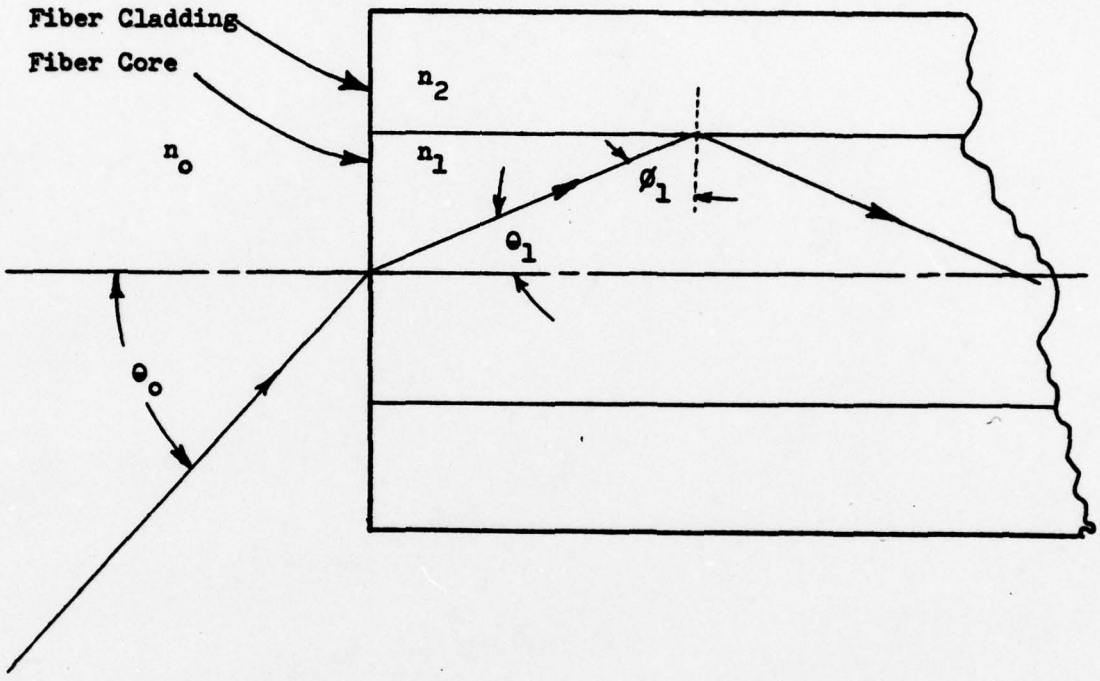

Figure 3. Angular relations for a ray of light being launched into an optical fiber. (From Kapany)[10]

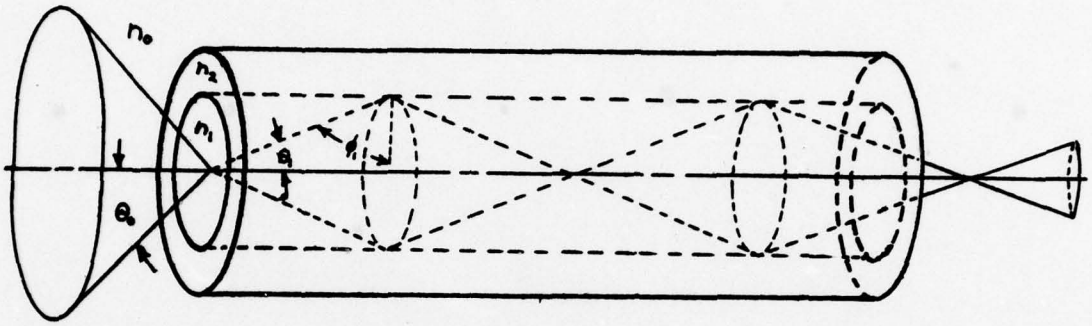

Figure 4. The cylindrical geometry of an optical fiber waveguide. (From Kapany)[15]

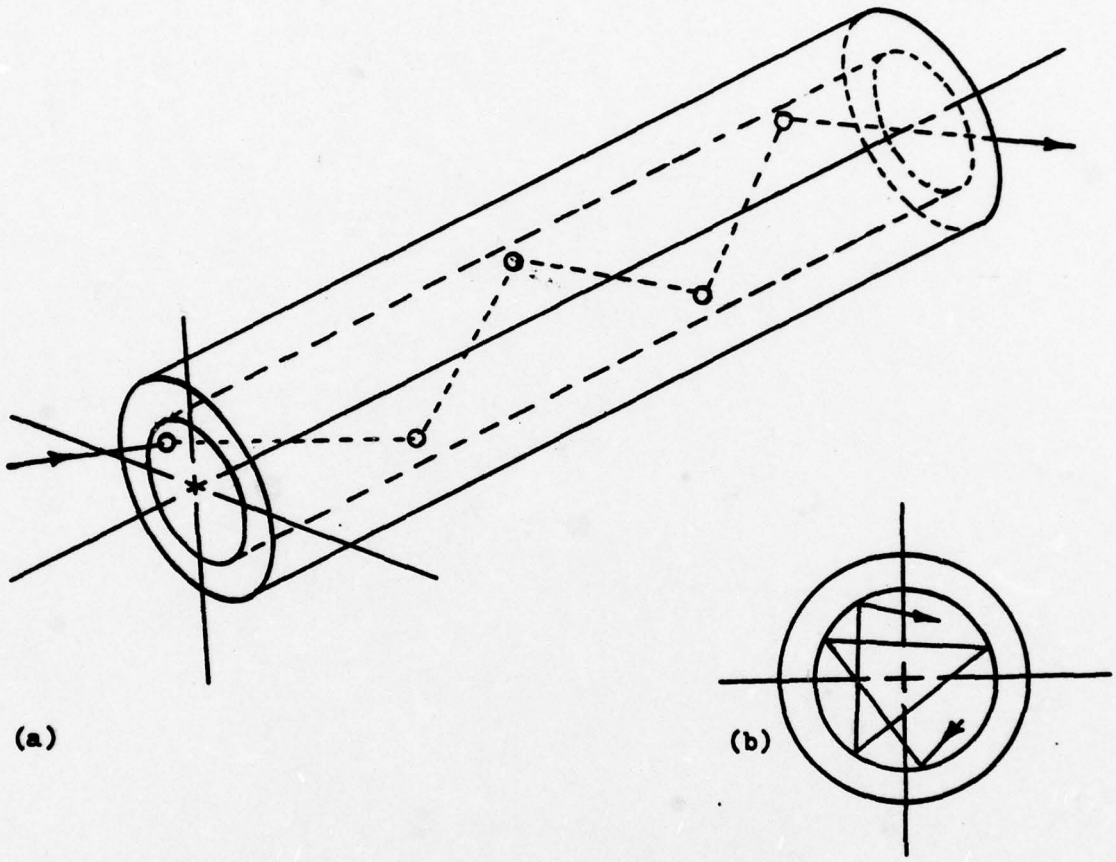

Figure 5. a) A skew ray traveling in an optical waveguide, b) helical path of the skew ray. (From Kapany)[16]

is much easier to understand and closely approximates the cumulative behavior of all rays present in the fiber.

The optical fiber is an electromagnetic waveguide, which will only allow certain modes to propagate. These modes can be considered as rays, each with a specific quantized value of Θ_1. The number of modes which propagate in a step index fiber can be calculated as:

$$N = 2(\pi a\ NA)^2 / \lambda^2 \qquad (6)$$

where a = the core radius, and λ is the wavelength of light which is propagating.[14]

Basically, there are three different ways in which optical fiber waveguides differ from each other. These are; 1) the material from which the fiber is made, 2) the size or more specifically the cross sectional dimensions, and 3) the refractive index profile.[17] Many different materials can be used to make optical fibers, but glass and plastic are by far the most popular. Some liquid cores have been used.[18] Many variations of material are possible, such as glass cladding on glass core, plastic on plastic, plastic on glass, glass on liquid, etc. Some fibers are unclad; more specifically they use the air around the fiber for the less dense medium.[19, 20]

For given values of refractive indices n_1 and n_2, which determine the numerical aperture, the size of the core radius governs the number of modes which will propagate at a given wavelength. This can be seen in equation (6).[21, 22] If the core radius is made small enough, only one mode will propagate and thus the fiber is called a single mode fiber. All other fibers are multimode fibers (See Figure 6). When the refractive index of the fiber is uniform across the core and is uniform across the cladding, but at a lower level, the fiber is said to have a step index profile. When the profile varies from a higher refractive index at the center to a lower index at its periphery, it is said to have a graded index profile. The core

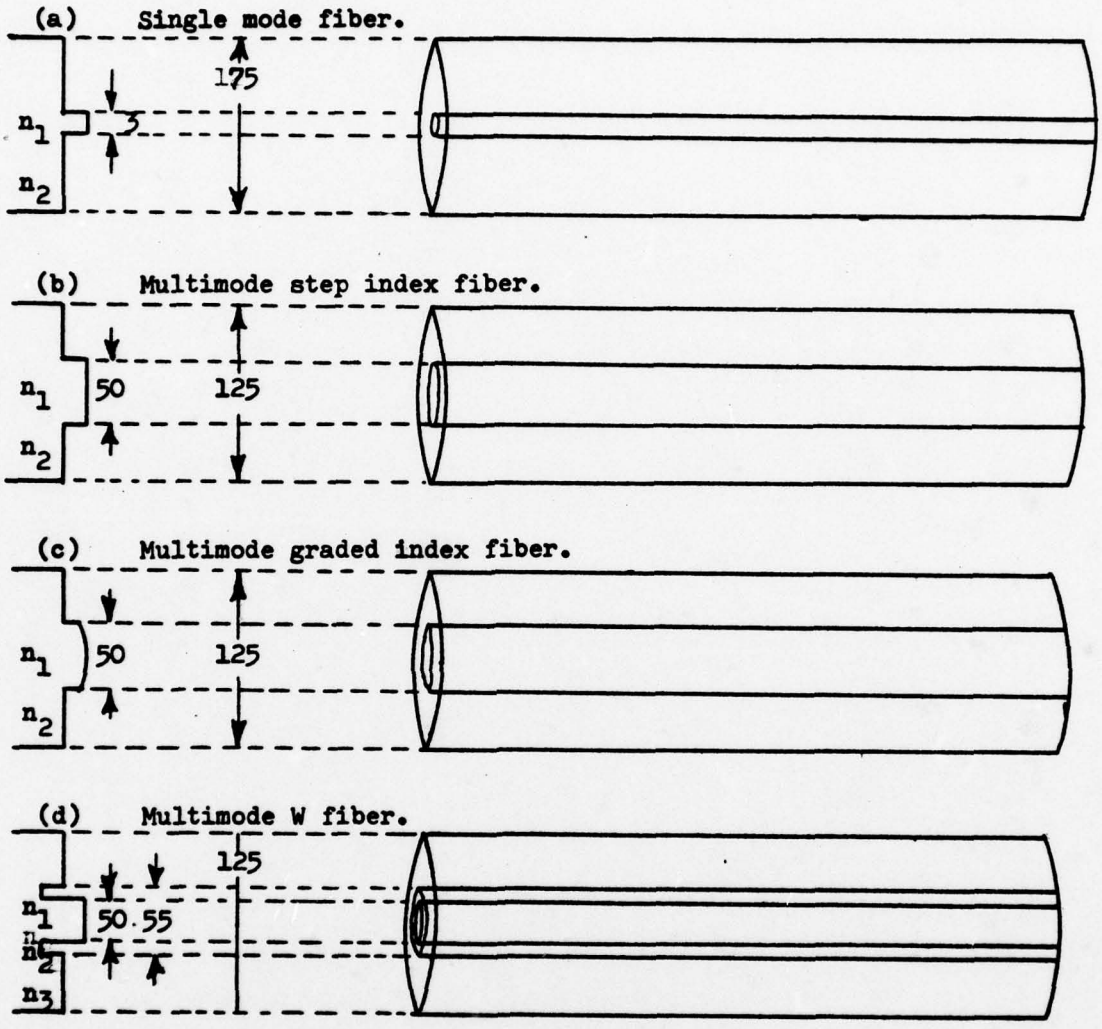

Figure 6. Types of fiber index profiles. (From Ramsay, Hockham, and Kao)[25]

index can be represented as:[23, 24]

$$n(r) = n_c (1 - 2\Delta(r/a)^{\alpha})^{\frac{1}{2}} \qquad (7)$$

where

$\Delta = (n_c - n_{cl})/n_c$,

$n(r)$ = the core index function,

n_c = the maximum index $n(r=0)$,

α = 1 to ∞ (2 for parabolic profile and ∞ for step profile)

n_{cl} = the cladding index.

For a given multimode step index fiber, the ray which propagates at the angle associated with the numerical aperture, travels a longer distance than a ray which travels parallel to the core axis. Since the core index of refraction is uniform, the first ray will take longer to traverse the length of the fiber than the second ray. When a light pulse is launched into a fiber, the pulse excites hundreds of modes in the fiber, each taking a different amount of time to arrive at the opposite end of the fiber. This broadens the pulse as it travels the length of the fiber. Pulse broadening is the mechanism which limits the bandwidth of optical fibers. With graded index fibers, as the refractive index decreases toward the periphery of the core, the propagation velocity increases so that the rays with longer path lengths travel faster. This limits the broadening, thus graded index fibers have larger bandwidths.[26]

Surveyed here were some basic concepts of optical fiber waveguides, including total internal reflection, refractive index profile, and numerical aperture. These concepts are used to describe misalignment loss mechanisms in optical fiber junctions (Section III) and the theory behind the three stub connector (Section V).

III. FIBER CONNECTION LOSSES

The first electromagnetic signals, being direct current on metalic conductors, encountered only resistive attenuation and negligible connector loss. Evolution brought about the low frequency alternating current signal (audio), which changed very little in the connector losses. Some reactive losses could be observed in connections but were still negligible in comparison to distributive losses.

As the telephone increased in popularity, the demand for trunk lines grew much faster than they could be constructed. The frequency multiplexed signal was the solution, but this required a higher frequency signal, with a bandwidth many times that of its predecessor, and as the signal frequency increases, the reactive losses increase. As the multiplex capacity increased, the conductors evolved through twin pair, spiraled pair, coaxial cable, metalic waveguide and finally to the state of the art, optical fiber waveguide.[27]

Along with this evolution the sophistication of connectors grew. At first, the major task was to cut down the reactive losses which had taken dominance over the resistive losses of previous connectors. Passing from the high microwave into the far infrared region, losses take on an entirely different nature. Although there are real and imaginary parts to these losses, they are usually not considered separately. Similar to connections at lower frequencies, optical fiber waveguide connections have some losses which are lumped representations of the distributed losses present throughout the conductor. Some of these are variations of cross sectional area, change in index of refraction profile, offset of the core axis relative to the cladding, and radiation due to bends in the fiber.

The distributive losses, or attenuation mechanisms, were categorized as either absorption or radiation by D. B. Keck. He concluded that these losses are

caused by either the material or the structure of the fiber.[28] Material absorption was the dominant attenuation mechanism throughout the infancy of optical fibers. Absorption in glass fibers occurs in three basic ways; intrinsic absorption of the glass, absorption by impurities, and absorption by atomic defects. Intrinsic absorption is caused by energy transfer to the glass. This is photon absorption in the ultraviolet region and vibrational or phonon transfer in part of the infrared. Neither of the regions affected is of main interest to communications applications.[29]

A more dominant cause of attenuation in glass is the transfer of energy to metal or hydroxyl ions, which exist as impurities in the material. It was found that as the impurities were reduced in glass fibers, the attenuation decreased at an amazing rate. This indicated that the impurities were responsible for much more of the losses than was the intrinsic absorption.[30]

Absorption because of atomic defects of the material is brought about by an external factor such as the thermal or radiation history of the material. Such absorption is usually avoided with the selection of a glass which resists such defects. However, this is of interest in military applications where radiation hardening is of great importance.[31]

One type of radiative loss is scattering, of which there are several types. Rayleigh scattering is caused by small changes in the index of refraction, from inhomogeneities in the material. These inhomogeneities are small compared to the wavelength of the light being propagated. Scattering caused by inhomogeneities of a size greater than that of a wavelength of light, are called Mie scattering.[32]

Changes in the fiber cross sectional dimensions or in the core to cladding index of refraction differential will cause power to be transferred from one propagating mode to another. Sometimes this transfer of power, or mode coupling as it is called, transfers power into radiating modes. This type of radiating loss

is called mode coupling scatter.[33]

A most interesting loss mechanism is that energy is radiated at bends in the fiber. Associated with a bend, is a radius of curvature and an origin for that radius. Since the fiber is bent, the electromagnetic field that travels along the edge of the fiber farthest from the origin of the bend, travels farther than that portion which follows the edge closest to the origin. If the bend is less than a critical radius, then somewhere along the fiber diameter the energy must propagate faster than the speed of light. It is at this point that the energy is no longer bound to the waveguide and begins to radiate.[34]

The proper end preparation of the fibers to be joined is an important factor in the reduction of losses. The fiber, like other products of glass, can break with one smooth plane which separates the two sides, or it can shatter with thousands of tiny faces, each oriented in a different direction. The second example is to be avoided since light incident upon each different face will be refracted in a different direction, and the original light will be refracted away from the fiber as loss. The proper end preparation, as described by Gloge, Smith, Bisbee, and Chinnock, yields a smooth, flat plane which is perpendicular to the longitudinal axis of the fiber. This method consists of bending the fiber on a smooth surface with a given radius of curvature, placing tension in the fiber, and scoring the fiber with a diamond edge. The radius of curvature, tension, and scoring pressure vary with the type of fiber. For silica glass fibers of 125 micron diameter, the radius of curvature should be 5.7 centimeters, with a breaking tension of 125 to 175 grams of weight applied to the fiber, and a scoring pressure of 1.5 to 7.5 grams applied to the diamond scribe.[35]

Another loss mechanism attributed to improper end preparation is that caused by fiber break angle. When the planar end of a fiber is not perpendicular to the longitudinal axis of the fiber it is said to have a fiber break angle. This angle is the deviation between the planar end of a fiber and a plane which is perpendicular

to the fiber axis.

Splice losses of this type were investigated by Gordon, Rawson, and Norton. If one fiber has such an angle, there will be an air gap in the joint between it and another fiber with no angle or a different angle. Assuming no other misalignments, light emerging from the end of the fiber with a break angle will be refracted by the air gap (see Figure 7). This refraction will tilt the emerging cone of light at an angle from the longitudinal axis of the two fibers. The cone of light emerging from the transmitting fiber no longer coincides axially with the acceptance cone for the receiving fiber. Because of this angular mismatch of transmitted versus acceptance cones for the respective fibers, some of the light entering the receiving fiber is beyond the critical angle for total internal reflection. This light passes right through the wall of the receiving core and is lost. For the most part, this loss disappears when index matching fluid is used in the fiber junction. Since the fluid fills the gap between the fiber ends and has the same (or close to the same) index of refraction, there is no (or negligible) refraction of the transmitted cone of light and subsequently all of the transmitted light is accepted by the receiving fiber.[36]

Since light propagates on an optical fiber as a guided wave, the alignment of two fibers at a joint is very critical. The three types of misalignment are longitudinal misalignment, angular misalignment, and transverse misalignment. These are also called end separation, tilt, and offset respectively. Figure 8 illustrates each of these misalignments.

Of the three misalignment losses, end separation is the least sensitive and easiest to control.[38, 39, 40] This aspect of end separation is more or less to be expected, since the divergence angle of the light exiting a fiber with proper end preparation is proportional to the numerical aperture of the fiber.

The numerical aperture is small for most fibers, (.11 to .48) but is espe-

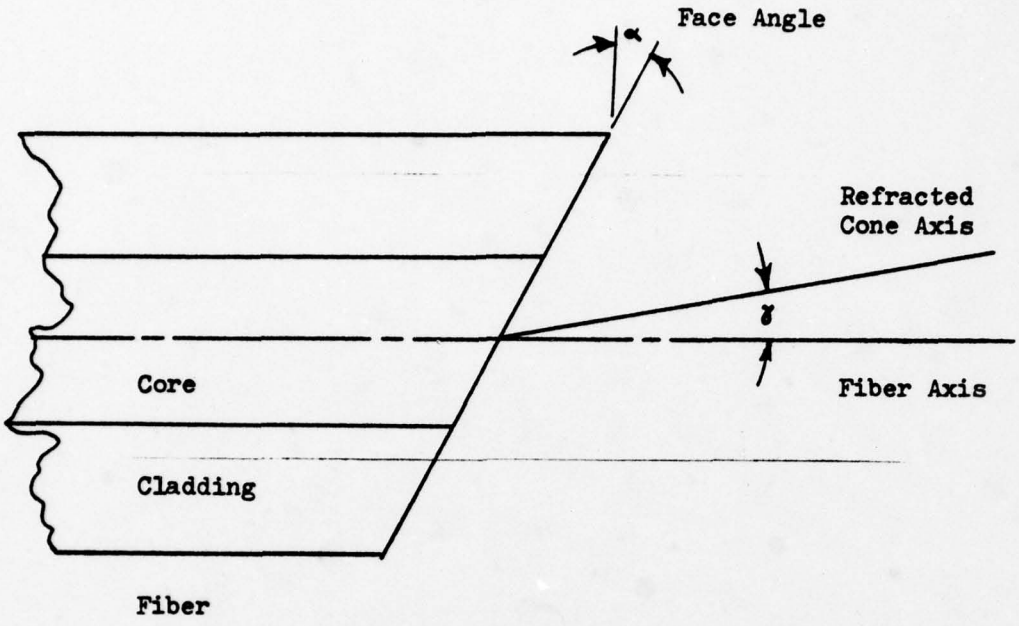

Figure 7. Relationship between fiber break angle and refracted cone axis. (From Gordon, Rawson, and Norton)[37]

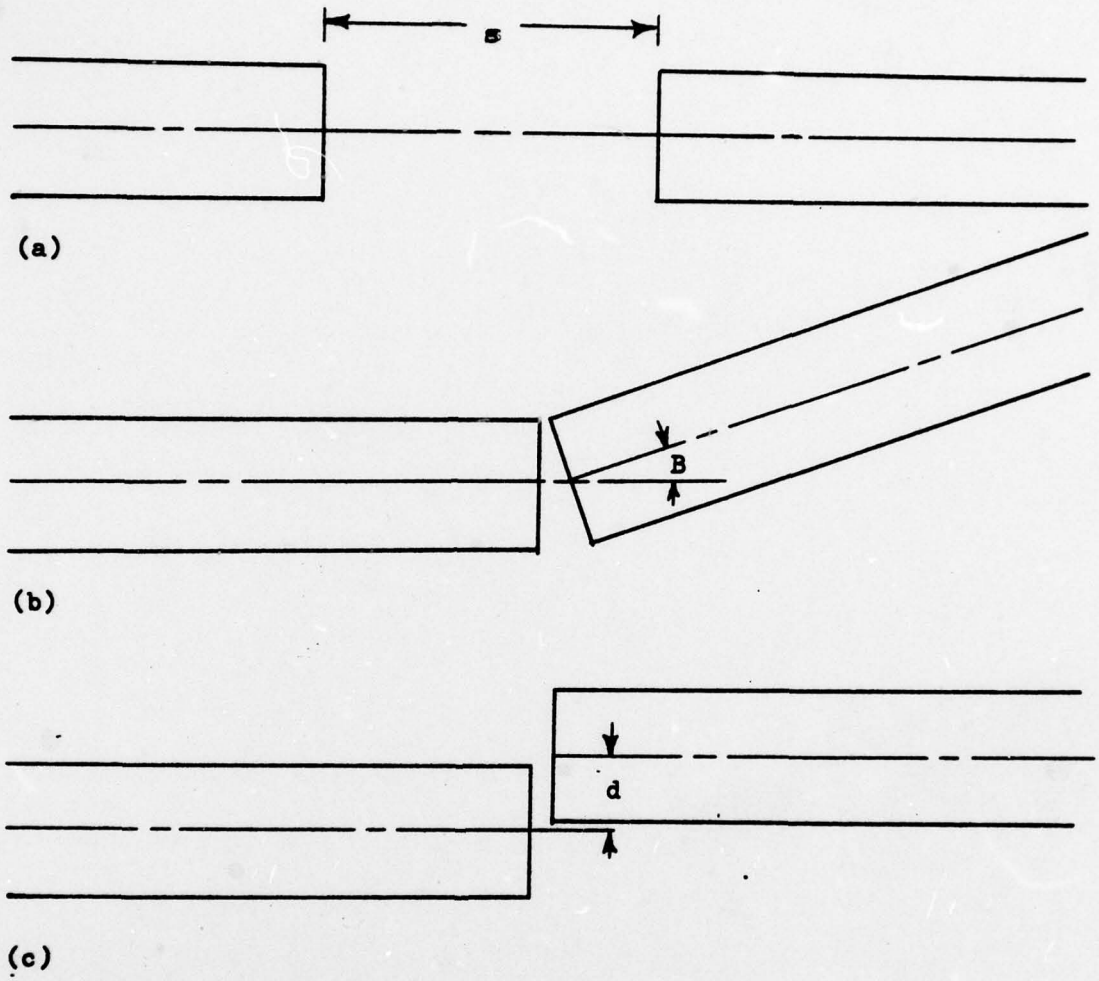

Figure 8. Fiber misalignments; a) end separation, b) tilt, and c) offset.

cially small for low loss fibers which are used in communications applications. Therefore, if the divergence angle of the emerging light is small, the beam width increases slowly with end separation. Therefore, loss increases more slowly with end separation, then it does with the other misalignment mechanisms.

Marcuse found that for single-mode fibers, a given fiber could be tolerant of tilt losses but intolerant of offset losses and for another fiber the opposite would be true. He expressed this as an uncertainty principle, where the specific tolerance is dependent upon the parameters of the fiber and the excitation pattern.[41] In most cases offset is accepted to be a more dominant loss mechanism than is tilt.[42, 43]

Figures 9 and 10 are the relationships, as reported by Chu and McCormick, for the three different misalignment losses. In these figures, s/R and d/R represent the normalized end separation and offset respectively, where R is the core radius, d the offset, and s the end separation. The angular misalignment α^{o} is normalized to the inverse sine of the numerical aperture ($\sin^{-1} NA_{o}$).[44]

Discussed in this section were some of the more dominant loss mechanisms which are present in optical fibers and fiber junctions. Many of these are material related, but offset, end separation, and tilt are attributed to misaligned junctions. Of these three mechanisms, it has been determined that offset is the mechanism to which optical fiber junctions are most sensitive. The intent behind the design of fiber couplers is to properly align the fibers, thus minimizing losses. In the next section a procedure will be presented to minimize offset misalignments in fiber couplers.

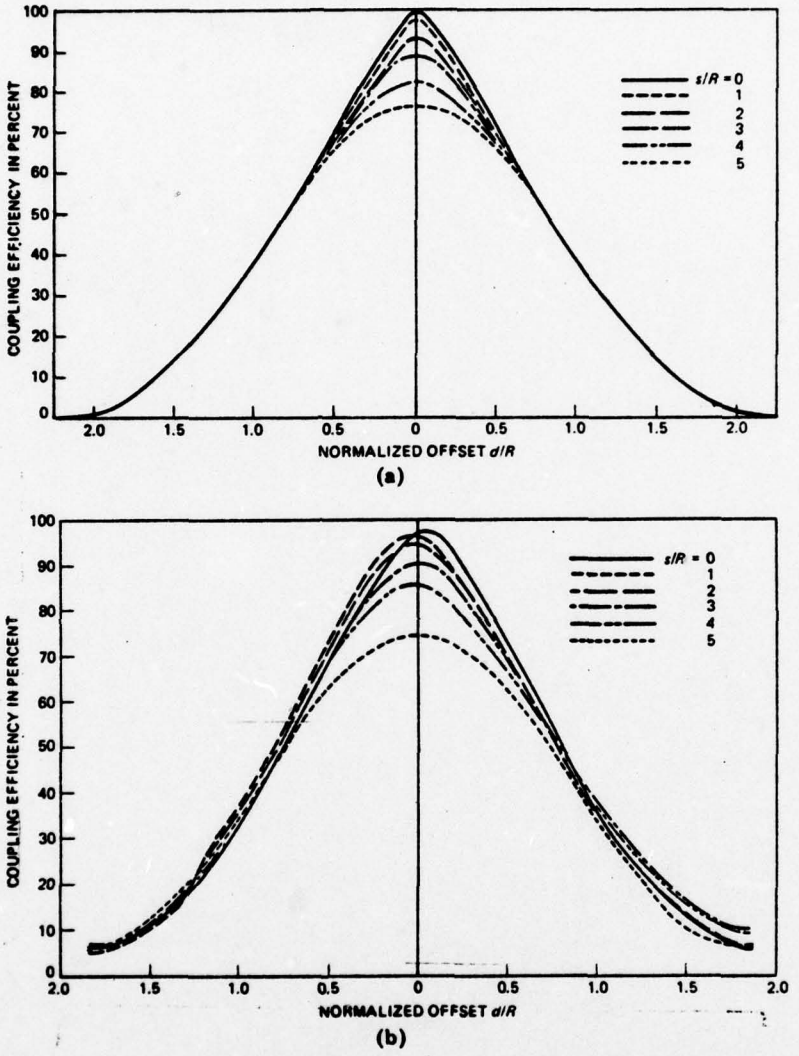

Figure 9. a) Coupling efficiency vs. normalized offset d/R at various separations s/R from the first experiment. b) Coupling efficiency vs. normalized offset d/R at various separations from the second experiment. (From Chu and McCormick)[45]

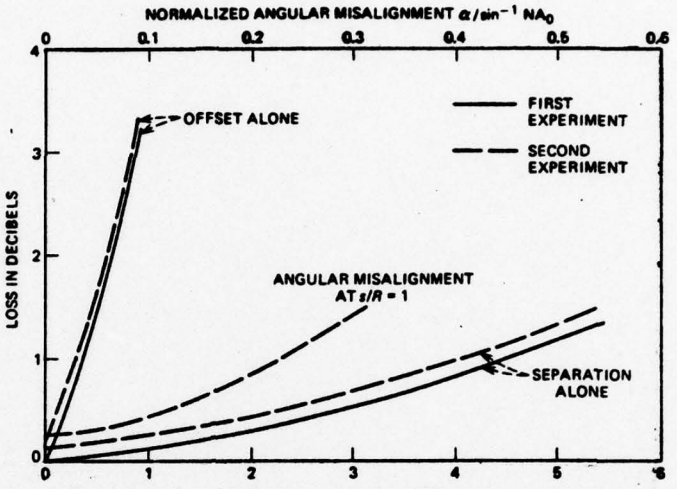

Figure 10. Loss in dB vs. normalized offset d/R, separation s/R, and angular misalignment $\alpha^{o}/\sin^{-1}NA_{o}$. (From Chu and McCormick)[46]

IV. THE THREE ROD GEOMETRY

As stated earlier, the three rod alignment technique capitalizes upon the geometry of three mutually tangent cylinders of equal radii, which form an interstice of exact proportions. Also, precision ground rods are easily obtained. This grouping of cylinders has the stability of an equalateral triangle. The interstice has exact dimensions which are independent of the forces holding the configuration in equilibrium.[47] (See Figures 11 and 12)

Another cylinder of radius equal to that of the original three divided by 6.464 can be placed inside the interstice. When the proportionality between this smaller cylinder and the original three is exact, the fourth cylinder is perfectly tangent to the other three. This smaller cylinder is then held rigid and parallel to the axes of the other three.[48] (See Figure 13)

This principle has been utilized in joining optical fiber waveguides.[49] Starting with two fibers of diameter (d), three cylinders of nomimal length are chosen with diameter (D = 6.464 d). The cylinders are held in the three rod bundle and the two fibers are inserted into the interstice from opposing ends of the bundle. Meeting in the center of the configuration, the fibers are perfectly aligned being that their cross sections are held perfectly rigid in the same position with respect to the same rods.[50]

In practice the alignment is somewhat less than perfect. First, the cylinders involved are deformable to some extent. Second, the diameter tolerances cannot be maintained exactly along any given fiber or from one fiber to another. In addition, an inward normal force must be maintained on the fibers from the rods, in order to keep the fibers from slipping out of the interstice. In order to do this, the holding rods are chosen such that their diameters are slightly smaller than

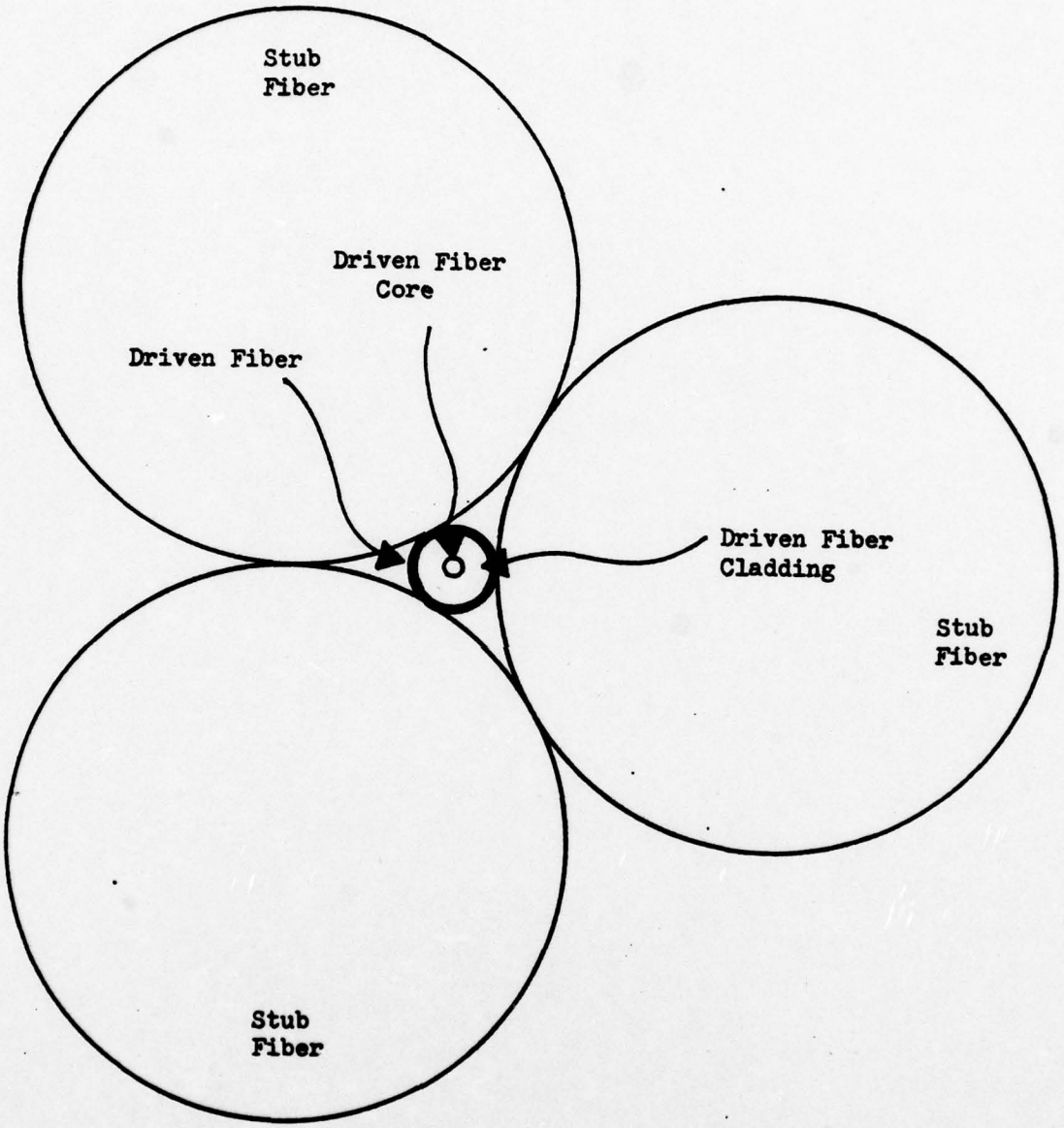

Figure 11. Coupler Face.

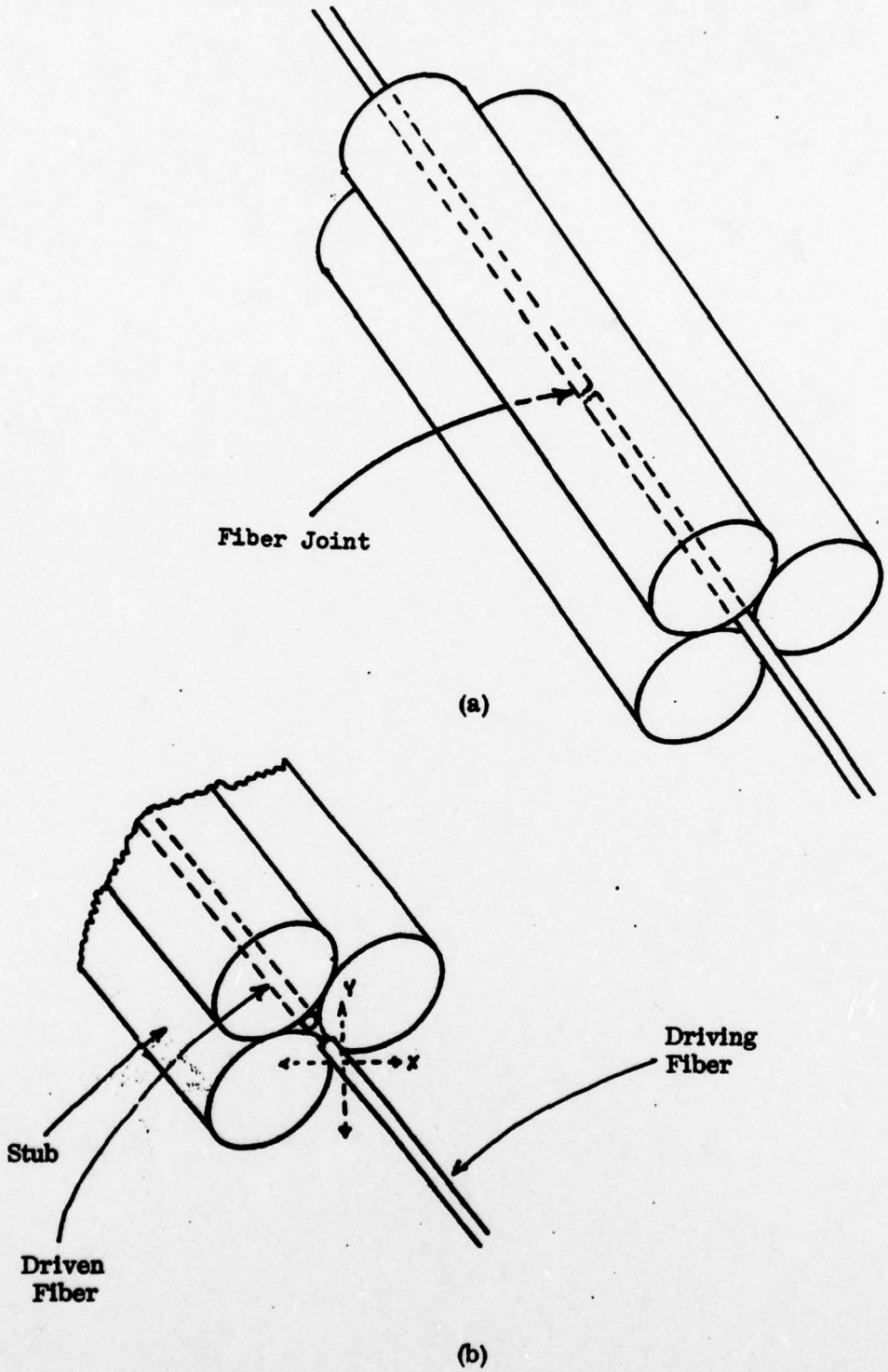

Figure 12. (a) The three rod fiber connector
(b) Three rod coupler

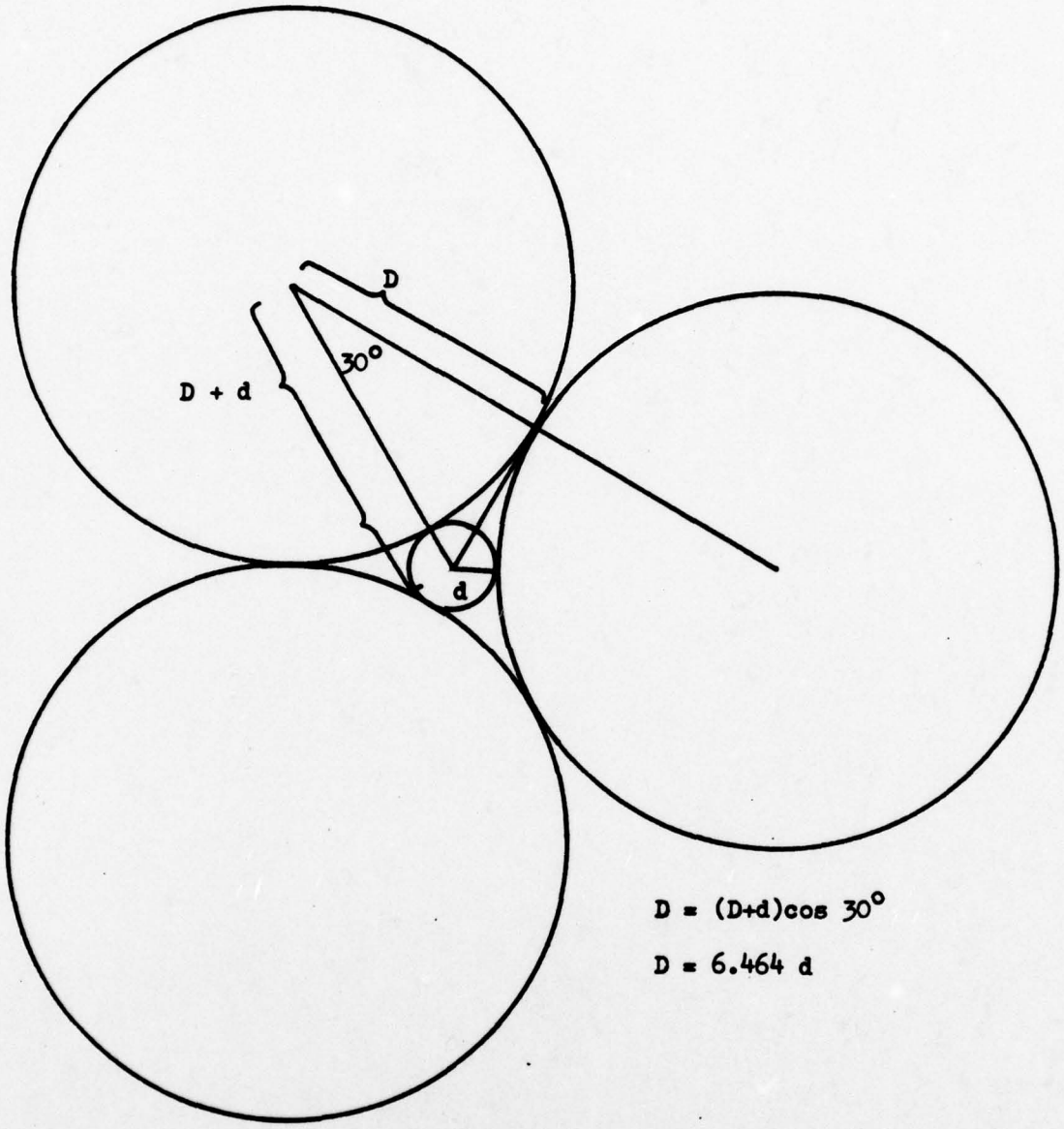

Figure 13. The three rod geometry.

required for the driven fiber. This holds the fibers tightly, but reduces the symmetry of the geometry and thus the alignment precision.

It is not the alignment properties that are of concern to this project, but only the geometry of the bundle. Instead of the alignment rods used to form the interstice, three optical waveguides are used. Now we have an optical fiber waveguide held in the interstice of three larger fibers arranged into the three rod bundle, where the end surface of each fiber has been properly prepared by accepted methods.[51] The four fiber ends are "butted" so that their end surfaces are all flush. (See Figure 11). This plane shall be called the coupler face. A piece of heat shrink tubing is then fused around the configuration to hold it rigid. The fibers are held parallel and rigid for a nominal length, determined by the power coupling requirements, and then allowed to diverge in any manner, dependent only upon the convenience of the application.

The type of fibers being mated (low loss) are characteristically of small diameter (i.e., 125 microns). To get a fiber with a diameter of over six times this value, medium or high loss fibers must be used. However, since only very short lengths are needed, the loss is not significant and plastic fibers with no cladding were used.

Given that the fiber to be mated has a diameter of 125 microns, the diameter of the larger fibers is approximately 31.8 mils. A circle containing the center of the faces of each of the larger fibers would have a radius of approximately 18 mils. We now want to mate an illuminated fiber of the same diameter with the center fiber of the four fiber configuration. For convenience the illuminated fiber will be refered to as the source, the fiber held inside the holding fibers as the driven fiber, the holding fibers as the stubs, and the combination of the driven fiber and stub fibers as the three stub coupler.

Rather simple conventional alignment techniques can be utilized to bring the face of the source into close enough proximity to that of the driven fiber that all of the illumination from the source falls within the circle on the coupler face which contains the three centers of the stub faces. The light falling within this circle must go into one or a combination of four places; the core of the driven fiber, the cladding of the driven fiber, one of the stub fibers, or vacant space in the interstice not occupied by the driven fiber. Ideally, all illumination from the source, assuming no cladding modes, will fall on the core face of the driven fiber. This is what should be achieved by optimising the connection.

If the incident illumination falls on one of the stubs, it can be detected at the opposite end of the stub and the source can be moved laterally away from that stub with an X-Y positioner of very good sensitivity, such as a differential screw.

If the source transmits light into the cladding, some of this light should be coupled into the stubs via the stub cladding interfaces. It is assumed, because cladding modes propagate as high order skew rays, that light injected into the cladding will result in equal intensity being coupled into each of the stubs.[52] This will be explained in more detail in the next section. In this manner, the X-Y positioner would first be "tuned" such that illumination appearing at the ends of the stubs is equalized among the three. This should bring the boundary of the source illumination pattern on the coupler face to within the circumference of the driven fiber cladding (this relation between the fibers is illustrated in Figure 18 of the next section). The next step then is to adjust the X-Y positioner such that the intensity in the stubs is minimized. Ideally this intensity should go to zero; however, in practice some error is expected. This procedure is explained in detail in Section VI.

The three rod geometry and the three stub coupler have been presented in this section. It has been proposed that by observing the power coupled to the stubs,

the three stub coupler can be used to maximize power transmitted through a fiber junction. A theoretical analysis of the operation of this coupler is discussed in the next section.

V. ANALYTICAL INVESTIGATION

The purpose of this analytical investigation is to predict the relative power lost as a function of offset misalignment between two optical fibers mated at a junction. Since only transverse misalignment was studied, the first assumption was that end separation and tilt losses are negligible. This assumption is considered reasonable because junction loss is less sensitive to end separation and tilt, and they can be more easily controlled through available technology than can offset. Experimental values of the lost power versus offset were measured with the coupler described in section IV. The experimental results are given in section VI, and are compared with the analytical results in section VII.

C. M. Miller developed a model to describe the radial offset dependency of the power percentage transmitted through the junction between two fibers. This was done for parabolic-profile fibers which closely approximate the graded index fibers used in this project.[53]

Miller started with three basic assumptions: 1) uniform power distribution is assumed across the core diameter of the source fiber, 2) the parabolic index of equation (7) is assumed for the fiber cores, and 3) the total power received at a given point is assumed to be limited by the lesser of the transmitting or receiving numerical aperture at that point.[54]

The numerical aperture, equation (5), as a function of radius becomes:[55]

$$NA(r) = (n(r)^2 - n_{cl}^2)^{\frac{1}{2}}. \qquad (8)$$

For fiber cores which have profiles described by equation (10), the numerical aperture as a function of radius becomes:[56, 57]

$$NA(r) = n_c\,(2\Delta)^{\frac{1}{2}}(1 - (r/a)^{\alpha})^{\frac{1}{2}}. \qquad (9)$$

The power accepted at any point (r) is:[58]

$$p(r) = p(O)\, NA^2(r) / NA^2(O), \tag{10}$$

$$= p(O)\,(1 - (r/a)^{\alpha}). \tag{11}$$

The total power in the fiber can then be calculated by performing an integration across the circular cross section of the fiber:[59]

$$P_T = p(O) \int_O^{2\pi} \int_O^a (1 - (r/a)^{\alpha})\, r dr d\Theta\,, \tag{12}$$

$$P_T = \pi a^2 \alpha\, p(O) / (\alpha + 2)\,, \tag{13}$$

where p(O) is a constant dependent upon the input power. The assumption of a parabolic profile sets $\alpha = 2$ and makes equation (13) take the following form:[60]

$$P_T = \pi a^2\, p(O) / 2\,. \tag{14}$$

For the problem of calculating the power transfer across the junction between two equal diameter but offset fibers, the locus of equal numerical aperture in the source and driven fibers is a straight line (see Figure 14). The cross hatched area in Figure 18 is the area where power will transfer between fibers. This is the area where two fiber end faces coincide. In region I the transmitting fiber has the smaller numerical aperture, and its function limits the power in this region. Integrating equation (11) over region I gives the following relation:[62]

$$P_I = 2\, p(O) \int_O^{\cos^{-1}(d/2R_T)} \int_{d_T/2\cos\Theta}^{R_T} (1 - (r/R_T)^2)\, r dr d\Theta\,. \tag{15}$$

In region II the receiving numerical aperture is the smaller. In order to integrate this region about the power distribution in the transmitting fiber it is necessary to translate the receiving numerical aperture to the center of the transmitting fiber. The result is:[63]

$$NA(r) = n_c (2\Delta)^{\frac{1}{2}} (1 - ((r^2 - 2dr\cos\Theta + d^2)/R_R^2))^{\frac{1}{2}}\,. \tag{16}$$

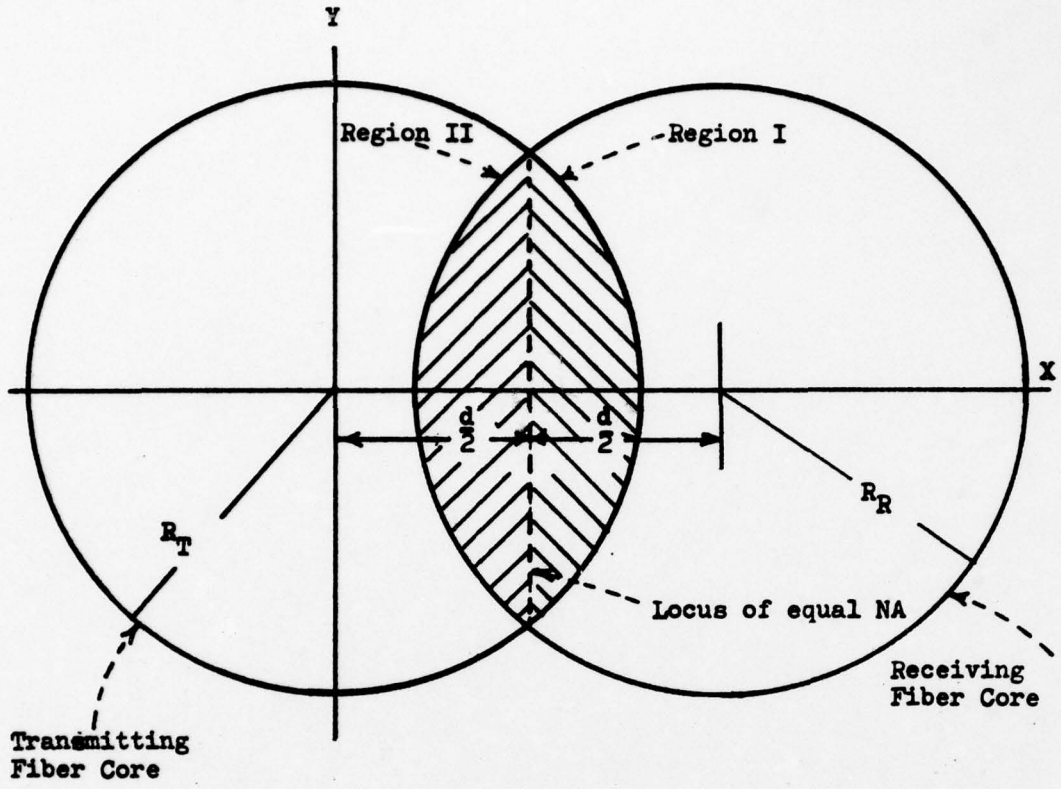

Figure 14. Overlapping regions of offset fiber cores ($R_T = R_R$)
(From Miller)[61]

For the assumed power distribution, the power transferred through region II is equal to that of region I. The percent power transmitted from one core to the other is then:

$$(P_I + P_{II} / P_T) \times 100\% = (2P_I / P_T) \times 100\% . \qquad (17)$$

A computer program was written to evaluate the above equation, and the results are shown in Figure 15. These results agree completely with those of Miller. Figure 15 displays, as did Miller, the calculated transmission, in percent, as a function of offset, normalized to the core radius. For the data of Figure 15 the computer was given a value of one for the core radius, and the offset was incremented from zero to two core radii in steps of two tenths. The program was also run for a core radius of 25 microns, and incremented at one micron intervals. The results are displayed in Figure 16 for offsets across the entire core face (from -50 microns to +50 microns).

Since the numerical aperture of the cladding is much larger than that of the core, it was assumed that all power lost by the core was captured by the cladding for displacements up to 37.5 microns. This value is the maximum displacement where the transmitting core will fall within the circumference of the receiving fiber's cladding. It was also assumed that the power in the transmitting fiber is entirely in the core, meaning that any cladding modes have attenuated to zero before the junction. With these two assumptions, the power percentage in the receiving cladding can be calculated by subtracting the percentage of power transmitted to the receiving fiber core from 100 percent. This calculation is displayed in Figure 17, which is thus a reflection if Figure 16, about the 50 percent line. After a displacement of 37.5 microns, the analytical description of the power in the cladding developed in this section is of little use to this investigation because light will begin to be coupled directly to the ends of individual stubs, and the power coupled to the

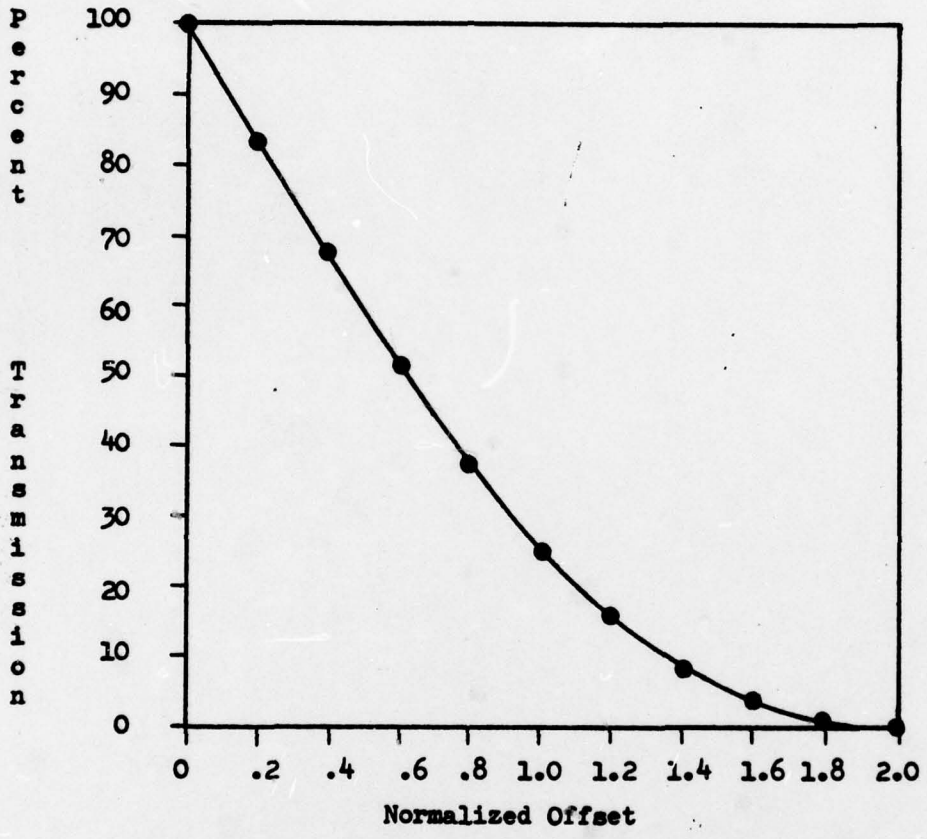

Figure 15. Calculated transmission in percent versus offset normalized to core radius.

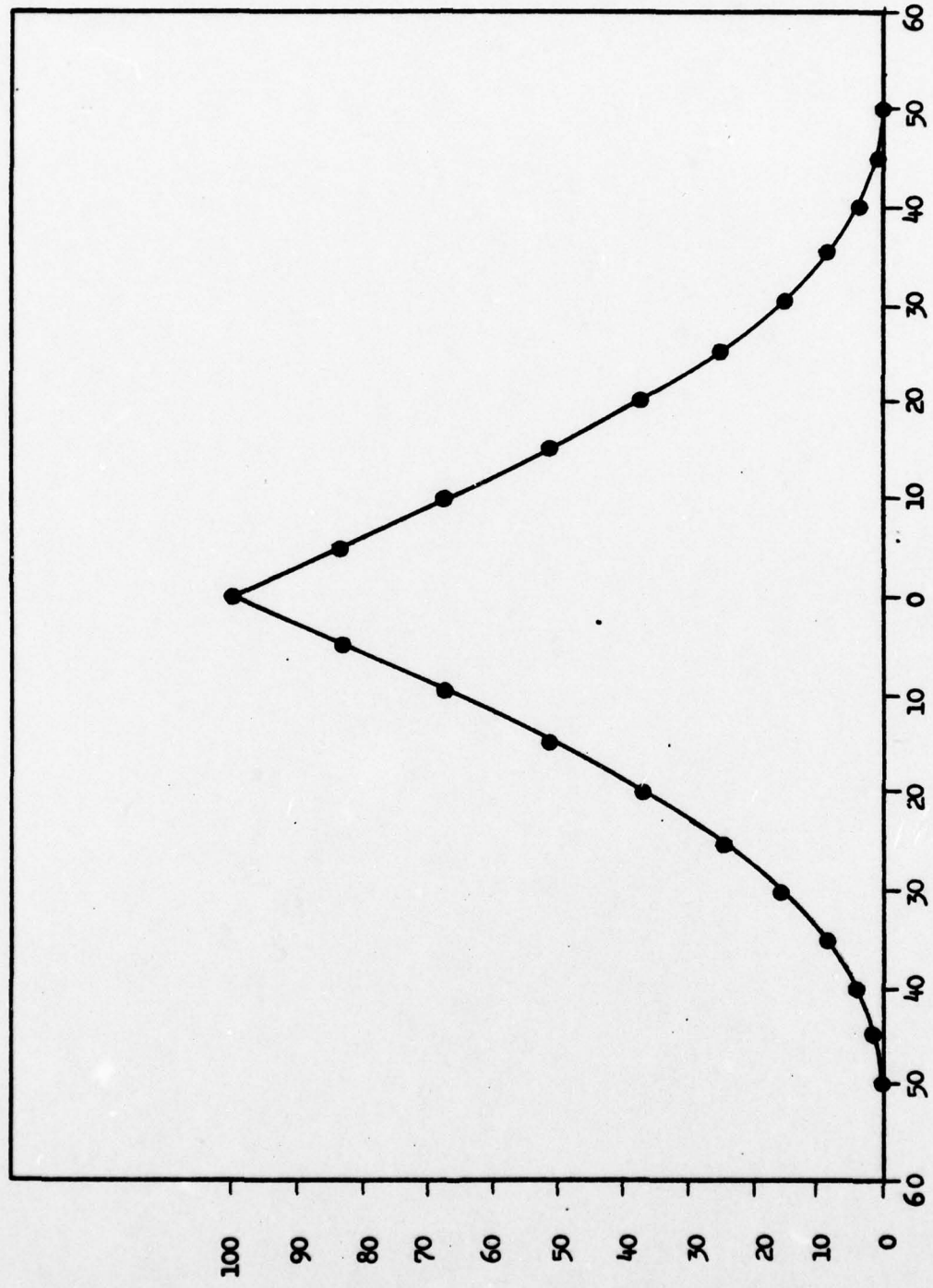

Figure 16. Calculated transmitted power in percent, versus offset in microns, for a parabolic profile fiber core of 25 micron radius.

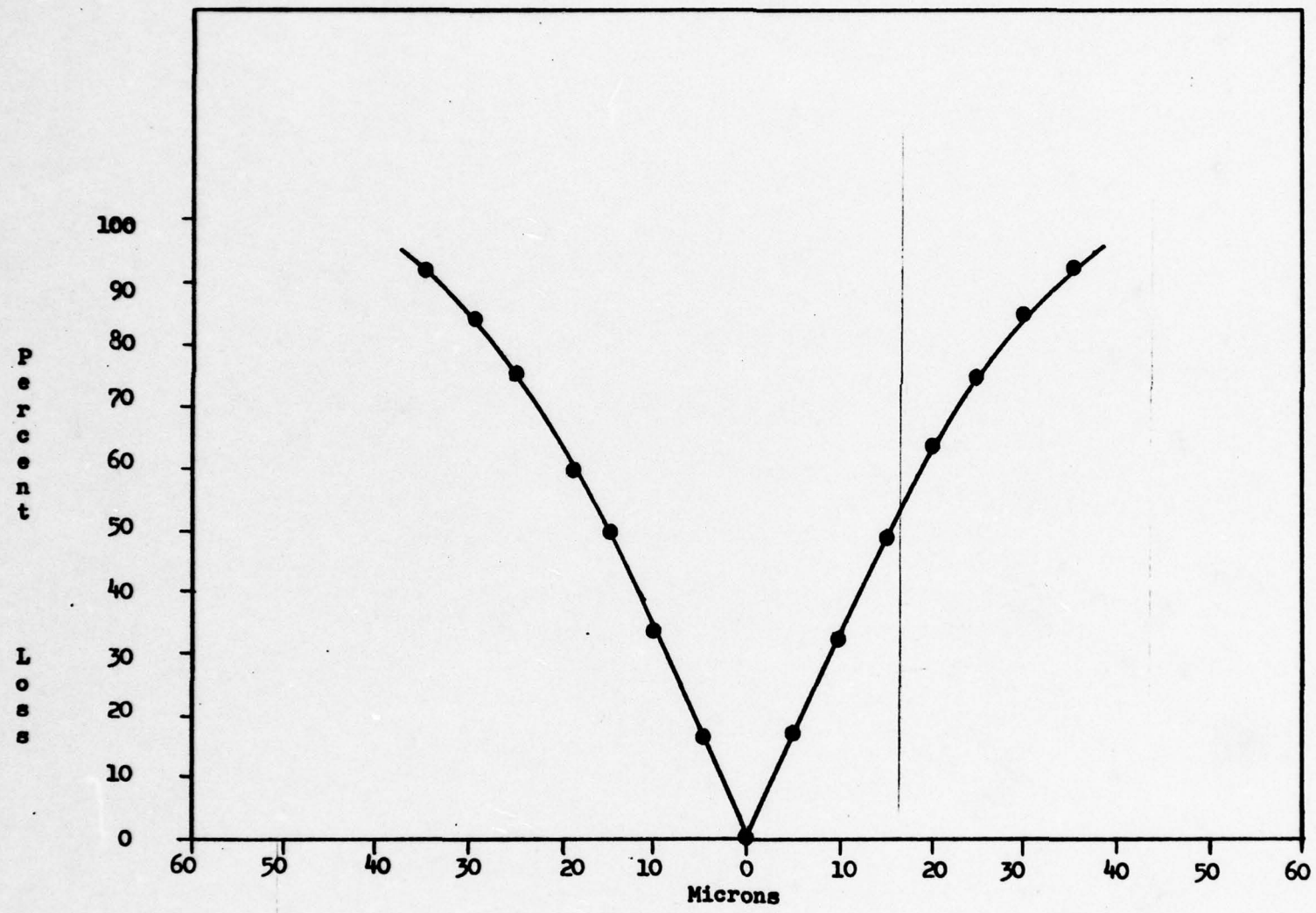

Figure 17. Calculated power lost to the cladding, in percent, versus offset, for a parabolic profile fiber core of 25 microns radius.

stubs will no longer be equal. It also becomes much more complicated to calculate. (See Figure 18).

An assumption is made that light entering the receiving fiber at any point on the face of the receiving fiber will, within a very short propagation distance (a few fiber diameters), assume a power distribution which is independent of the angular component of the radius vector to the point of entry. In other words, light entering a fiber off axis will, within a very short propagation distance, assume a power distribution which is circularly symmetric about the longitudinal axis of the fiber. In support of this assumption, Kapany observed that the conduction property of an optical fiber is dominated by light rays which are skew to the axis of the fiber. These skew rays propagate in a helical path as they are reflected by the cylinder walls (See Figure 5).[64] Since the coupling lengths that were used in this project were very large compared to the diameter of the fiber, it is reasonable to assume that most rays have rotated about the fiber axis very many times within a coupling length. Furthermore, Jeunhomme and Pocholle reported for fibers of one meter in length, that the output field patterns were dependent upon the length of the radius vector to the point where light passed through the entrance face of the fiber, but were <u>independent</u> of the angular component of this radius vector.[65]

By referring to Figures 11 and 18, it can be seen that any light entering the larger stub fibers prior to a displacement of 37.5 microns must come through the sidewalls of the receiving fiber cladding. The transverse coupling of light between two fibers has been given much attention because of its application to conductor crosstalk. Unfortunately, these applications assume very long coupling lengths (greater than ten meters), and coupling between fibers of identical dimensions and composition. For that application, coupled mode theory can be used with rela-

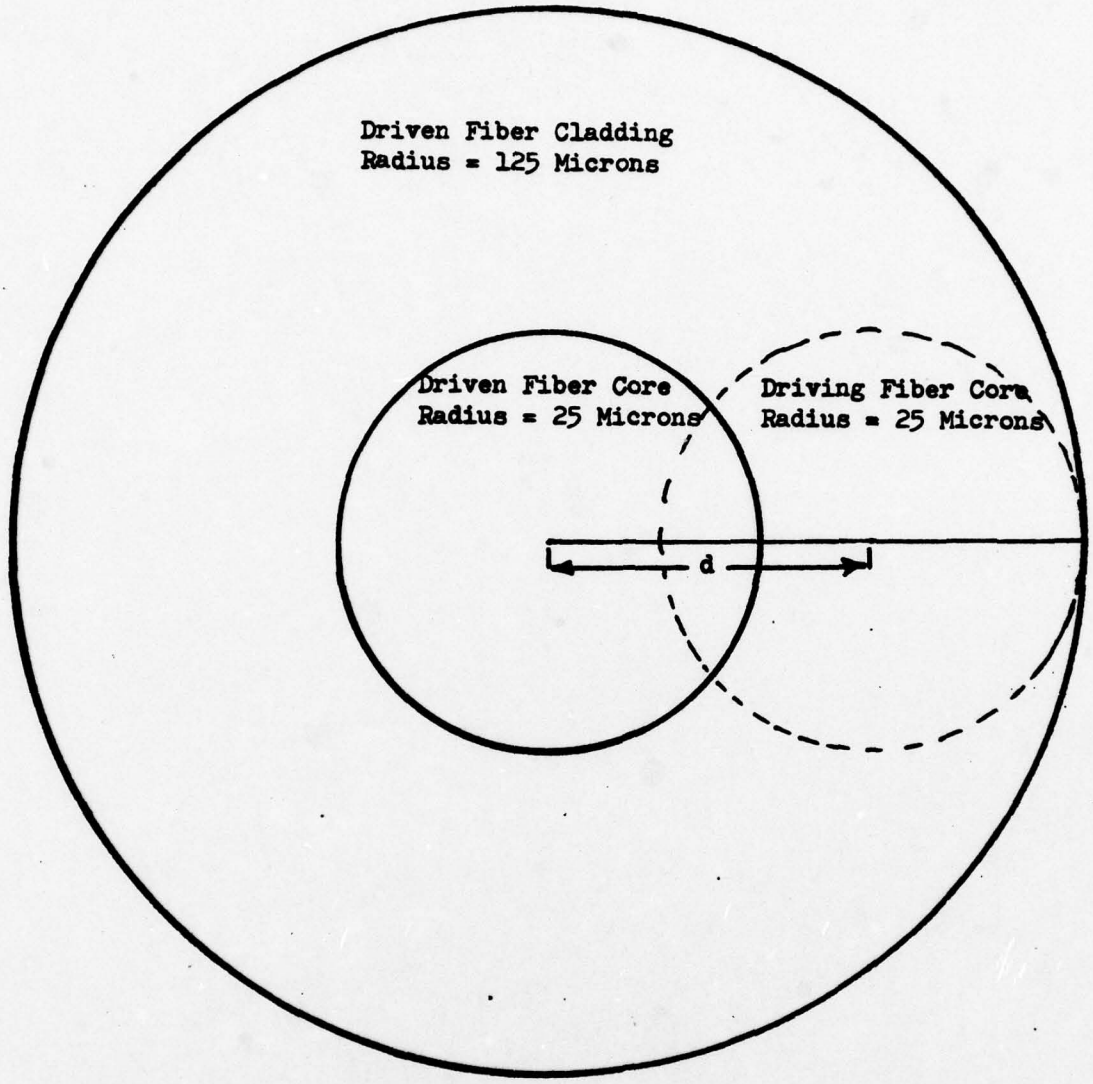

Figure 18. Driving fiber core displaced by d = 37.5 microns, along radial line $\gamma = 90^{o}$. 37.5 microns is the maximum displacement where light from the driving fiber core falls within the periphery of the driven fiber cladding.

tive ease because identical modes exist in both fibers.[66] McIntyre and Snyder have reported coupled mode relationships for fibers of arbitrary dimensions and dielectric constants. However, they still assume small values of delta (δ) where:

$$\delta = 1 - (n_{cl}/n_c)^2 \ .$$

This assumption is very applicable for coupling between cores of two communications fibers, because by design, the delta is small for each.[67] In this project, the energized fiber core is the cladding of the receiving fiber and its cladding is air. The non-energized fiber, the one to receive the transverse coupled power, is a plastic unclad fiber, again with air for the cladding. Both cases result in relatively large deltas.

A mechanism which better explains the transverse coupling in its application to this project is that of frustrated total internal reflection. Cherin and Murphy have used this method to successfully predict crosstalk between optical fibers. Recalling Figure 2, a ray is totally reflected for values of $\emptyset$ which exceed $\emptyset_c = \sin^{-1}(n_2/n_1)$, when n_2 is greater than n_1. The amplitude of the electromagnetic field decays exponentially in the medium with the lower index of reflection. However, the Poynting vector is not equal to zero in the rarer medium, only its time average vanishes. Strict geometric optics dictates that the ray reflects instantaneously at the boundary between the media. The actual power flow is shown in Figure 19, which also illustrates that smaller $\emptyset$ penetrates deeper past the media boundary. This representation also explains the Goos-Hanchen shift (d) between the reflected and incident rays.[68]

If a third media is brought into proximity to the boundary from the side with the smaller index (n_2), some of the energy can be trapped in the third media dependent upon $\emptyset_1$ if n_3 is greater than n_2. Some of the energy will be trapped

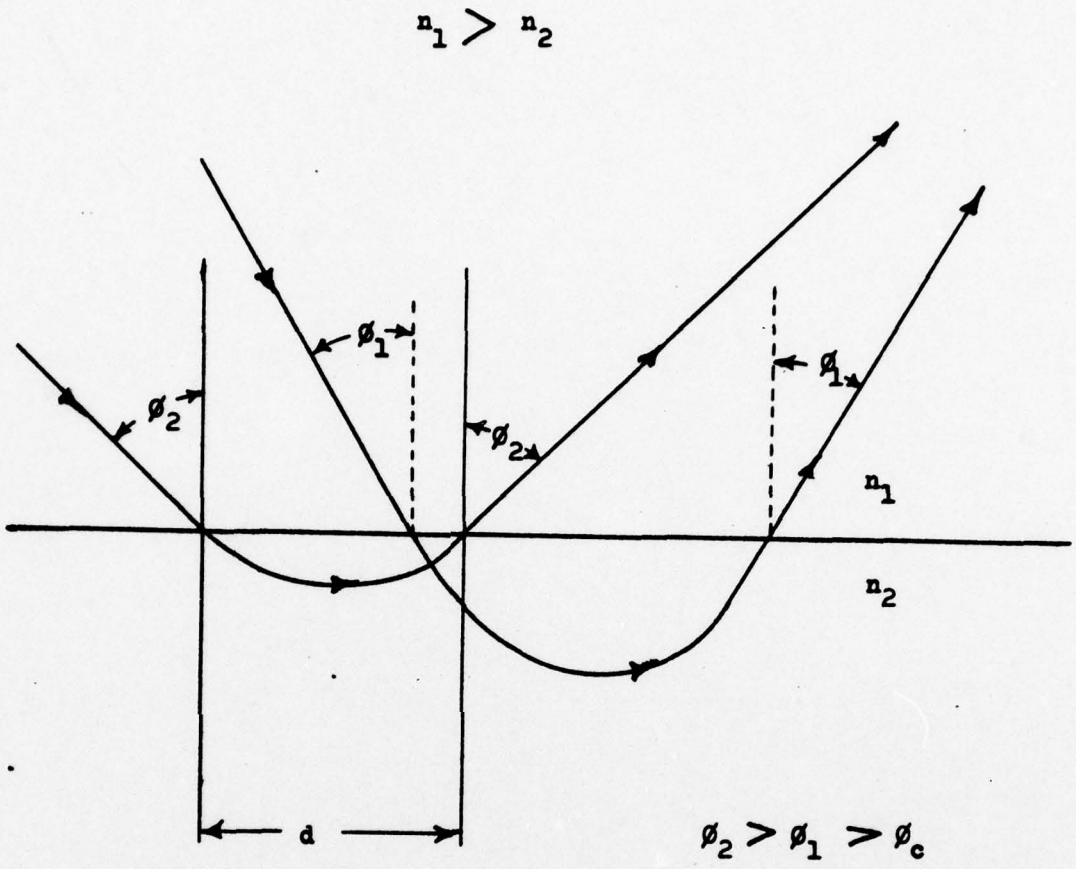

Figure 19. Displacement of light ray upon reflection. The Goos-Hanchen shift. (From Cherin and Murphy)[70]

for any value of $\emptyset_1$ if n_3 is greater than n_1 (See Figure 20). This energy trapped by frustrated total internal reflection, then propagates in the third medium as a ray of light. If the separation between medium number 1 and medium number 3 should close to the point that they actually touch, energy is transferred directly into medium number 3 as a refracted ray. This transfer is governed by the laws for refraction from basic physics.[69]

Figure 21 shows that at the point where the two fibers touch, light rays are transferred across the boundary as refracted rays. In regions on either side of that point, the frustrated total internal reflection mechanism is in operation. Strict geometric optics would predict power transfer only at the point of contact. Electromagnetic field theory predicts power transfer for points where the separation is small but non-zero. The amount of power transferred is dependent upon this separation. Power is then transferred between fibers throughout the arc (w) instead of only at point (p).[73]

At this point transmission coefficients could be derived to describe more accurately the power transfer between the fiber. The results, however, would be only as reliable as the description of the light propagating in the receiving fiber cladding. It has not been possible at this point to adequately describe this energy. The transfer mechanism has been described enough to predict a direct proportionality between the power in the receiving fiber cladding and the power in the stub fibers. This proportionality is direct and it is expected that as the displacement increases up to d = 37.5 microns the power in the stub fibers will also increase. Also, if the angular nondependency assumption holds, the relation between power collected in the stubs and radial displacement is the same for radial displacement in any direction, independent of the stub positioning.

After the radial displacement has surpassed 37.5 microns, the power in the

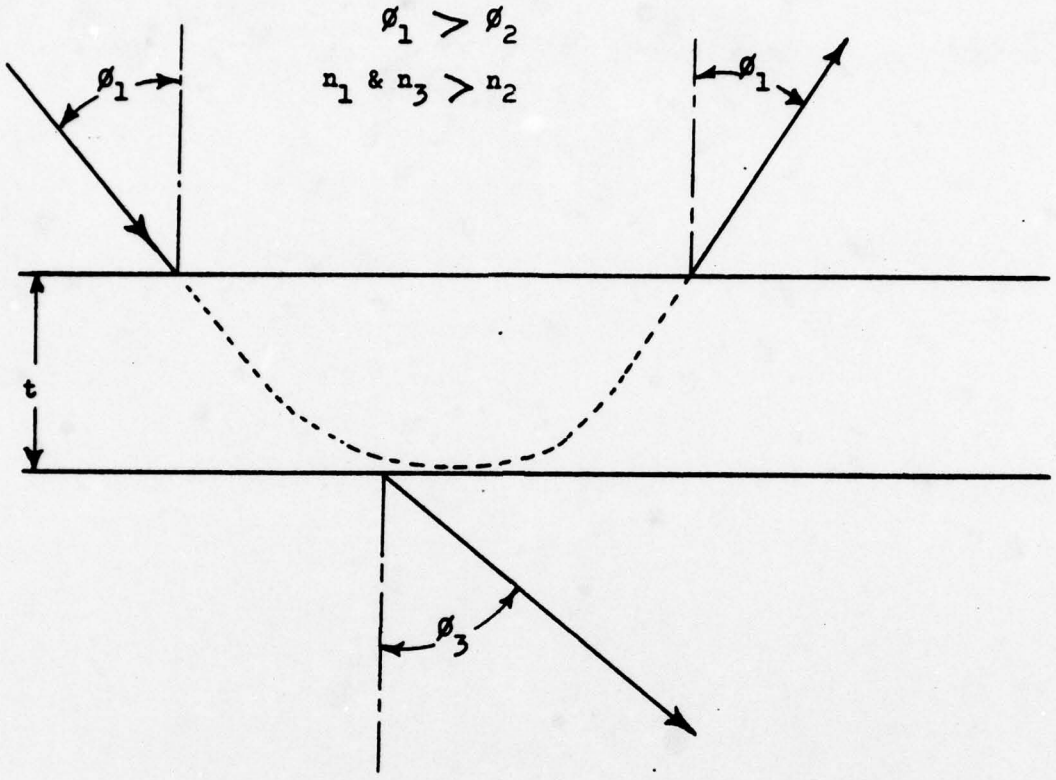

Figure 20. Frustrated total internal reflection of a light ray. (Cherin and Murphy)[71]

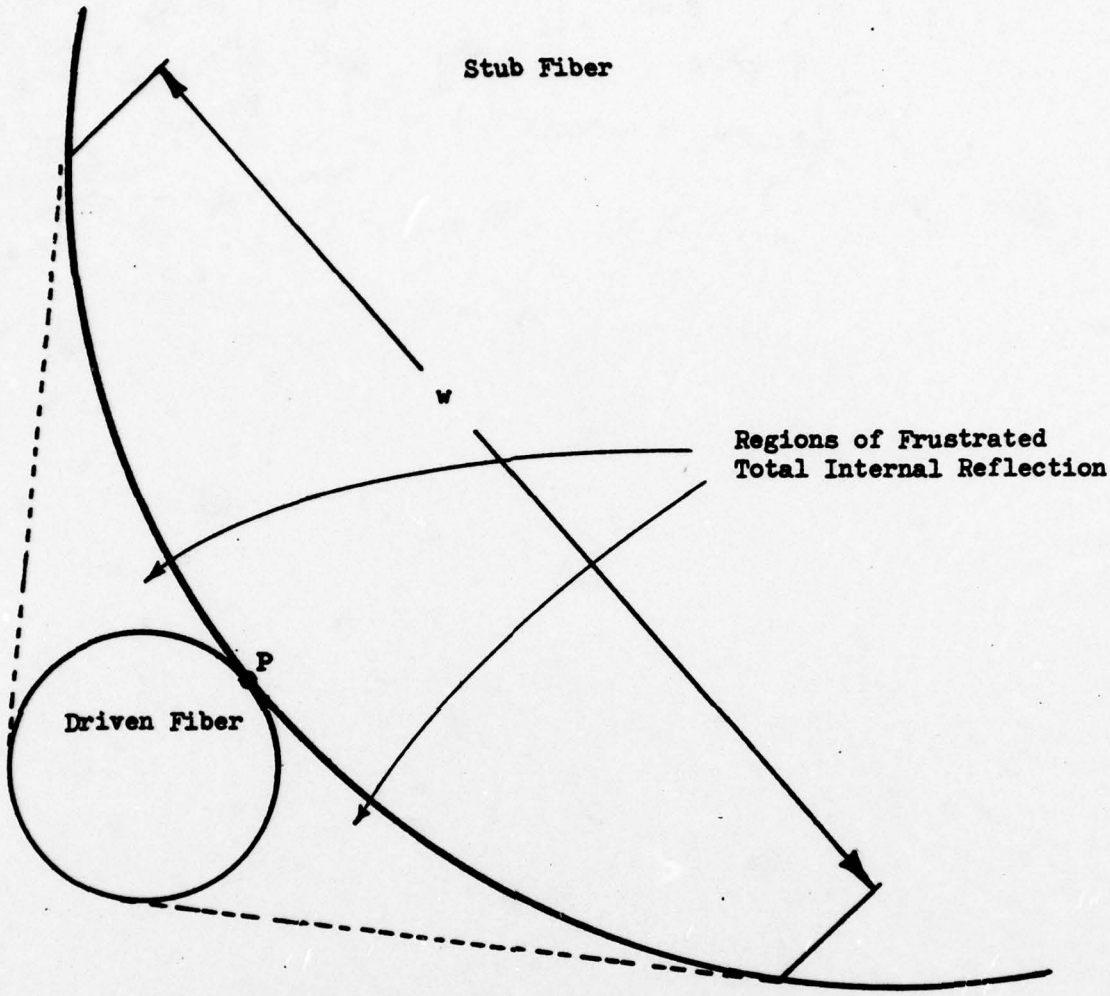

Figure 21. Regions of frustrated total internal reflection for the Stub Coupler geometry.[72]

stubs is dependent upon the direction (γ). Because of the three rod geometry, this dependency repeats every 120° and only needs to be described through a rotation of 120°. At $\gamma = 0^{\circ}$, the transmitting fiber begins to launch directly into the end of stub number one as the radial displacement increases above 37.5 microns (See Figure 22). With increasing displacement and $\gamma = 0^{\circ}$, the power in stub one increases at a rate much faster than stubs two and three. The power in the stubs is no longer equal. After a displacement of 50 microns the power in the receiving fiber cladding has started to decrease, and with it the power in stubs two and three. After a displacement of 87.5 microns all of the power in the transmitting fiber core is launched into stub one. No power is launched into the receiving fiber and likewise, since no power is present in the receiving fiber cladding, the power in stubs two and three is zero. The relative proportionality between the power in each of the stubs and the displacement is illustrated at Figure 23. The exact proportionality is not known, but the increasing and decreasing trends are indicated.

For $\gamma = 60^{\circ}$, power is launched into the interstice between the driven fiber and stubs one and two. This interstice is not a guiding channel, since the fibers that make up its boundaries have higher indices of refraction than the interstice. Hence, there is no total internal reflection. For this reason, any power launched into the interstice is refracted into the driven fiber's cladding or stubs one and two. The stubs make up more of the boundary of the interstice than does the driven fiber, and will receive more of the refracted energy. As the radial displacement along $\gamma = 60^{\circ}$ increases past 37.5 microns, the power in stubs one and two increase and the power in stub three decreases.

For $\gamma = 120^{\circ}$, the same relations hold as for $\gamma = 0^{\circ}$, except that stub two assumes the role of stub one, stub three becomes two and stub one becomes three. For values of γ between 0° and 60°, varying combinations can be expected between

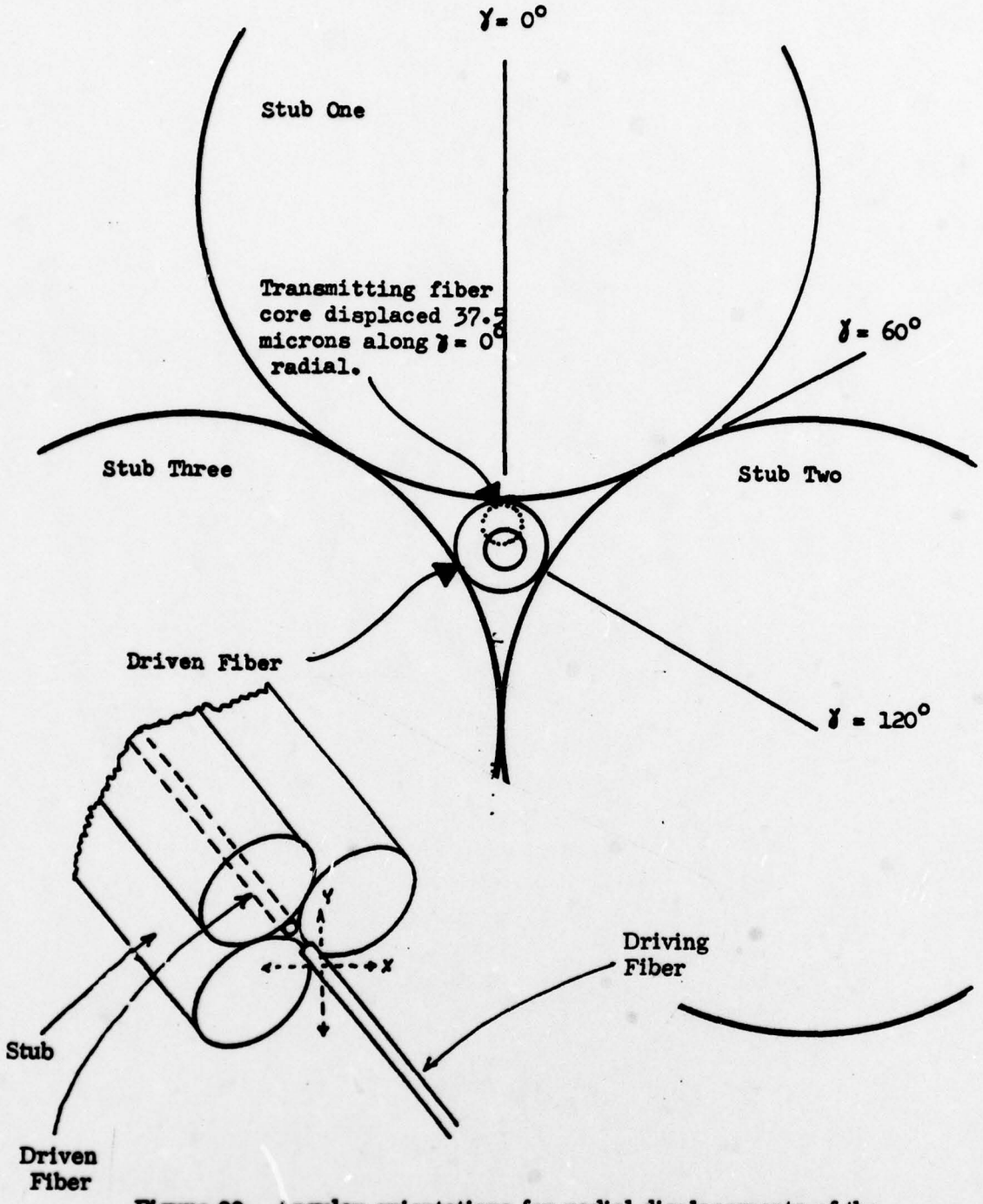

Figure 22. Angular orientations for radial displacements of the transmitting fiber core on the coupler face.

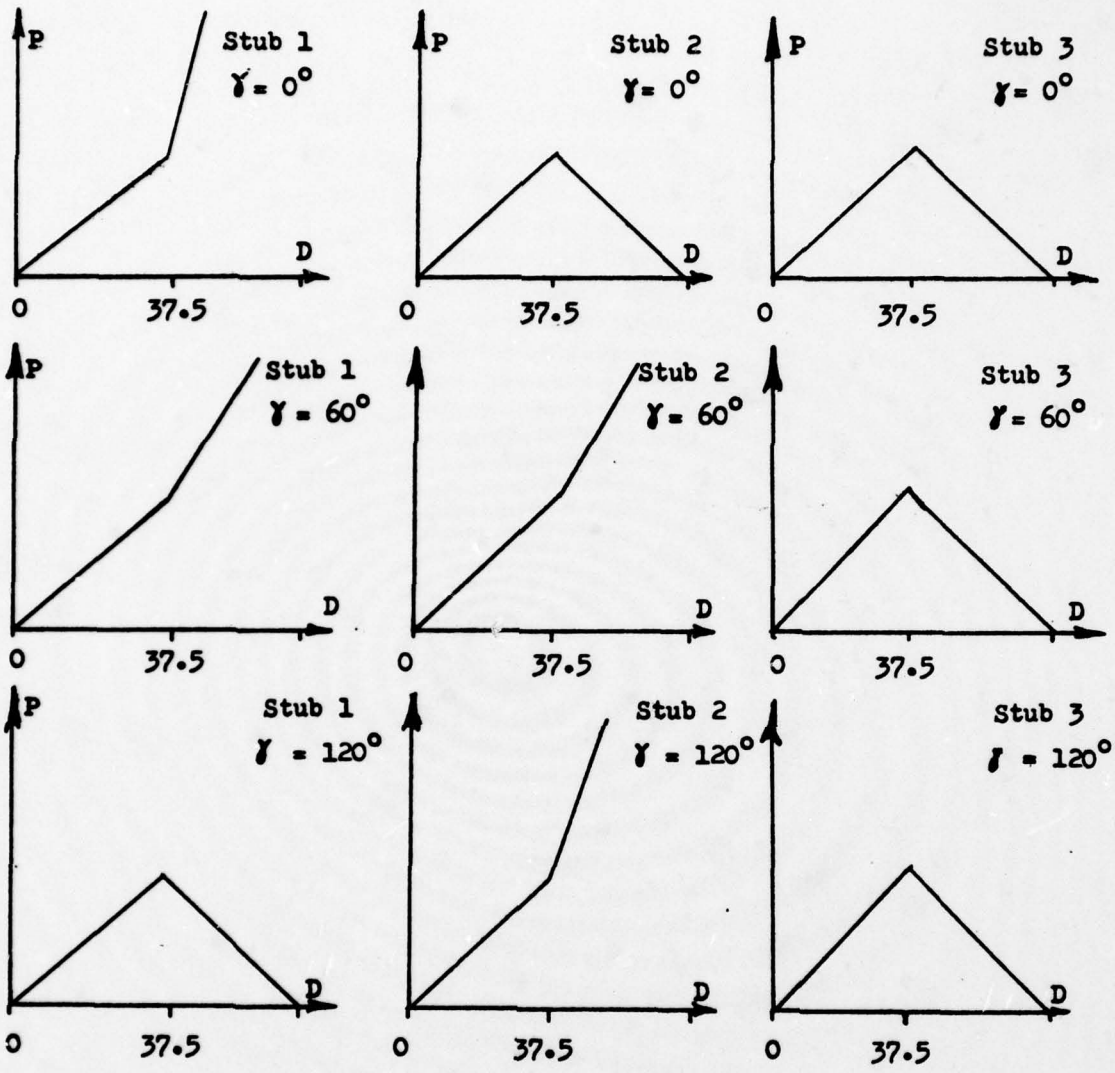

Figure 23. Estimated trends of stub power versus radial displacement for radial orientations of 0°, 60°, 120°.

the power relations of $\gamma = 0^{\circ}$ and $\gamma = 60^{\circ}$. Similar variations hold for values of γ between 60° and 120°.

From the foregoing arguments, no quantitative results were predicted, only predicted trends of increasing or decreasing power levels, dependent upon radial displacement. A summary of these predicted trends follows:

--- For radial displacements greater than 37.5 microns, the relative position on the coupler face can be identified by the differing power levels of the stubs.

--- For radial displacements less than 37.5 microns, the power levels in each of the stubs will be equal, and will vary identically for radial displacements in any direction.

--- The power in the stubs all decrease to zero as the radial displacement decreases to zero.

The three stub coupler, which maximizes power transfer through a fiber junction by minimizing the fiber offset, was presented in section IV. A theoretical analysis of the coupler's operation was discussed in this present section. Section VI describes the experimental analysis of the coupler and tabulates the results of that analysis.

VI. EXPERIMENTAL INVESTIGATION

The basic strategy of the experimental investigation of this project was to build the coupler described in section IV, and measure the power levels in the driven fiber and the stub fibers. After observing the correlation between the degree of offset and the power distribution between the stubs, a scheme was developed to maximize the power through the junction by adjusting the offset until the stubs showed a minimum power level.

It has been found that an optical fiber of the type used in this project will not assume its steady state power distribution until a length of 1.2 kilometers has been reached. For this reason, each length of communications fiber used should have a length of at least 1.2 kilometers to adequately simulate actual operating conditions.[74] Cost prohibited the use of such lengths of fiber so shorter lengths had to be used. One of the problems with shorter lengths of fibers is the presence of cladding modes, that is, light guided in the cladding. These modes are excited at every source, every fiber junction, and to a lesser extent, along the fiber itself because of the misalignments, impurities, and changes in the fiber dimensions. Since the outside cladding surface has many more impurities than the core to cladding boundary, and since most fibers are covered with a lossy jacket, cladding modes attenuate much faster than do core modes. Fibers are designed with a lossy jacket next to the cladding to attenuate cladding modes because the presence of cladding modes would increase the pulse broadening and thus decrease bandwidth. The short lengths of fiber used in this project did not attenuate the cladding modes sufficiently, so cladding mode strippers were used to help eliminate some of this unwanted energy. A mode stripper is constructed by removing the protective jacket from a length of fiber to bare the cladding surface, then immersing it in

an index matching liquid. The index matching liquid is either of the same refractive index or a higher index than the cladding. As a result, total internal reflection no longer exists at the cladding surface and the cladding modes escape.

A schematic diagram of the experimental apparatus is at Figure 24. A helium neon laser was used for the light source. Slight variations in power caused the light intensity to vary slightly (maximum of 5%). Light from the laser was focused through a 10X microscope objective unto the face of a 125 micron diameter fiber of approximately 40 meters in length. The last four feet of this fiber was stripped of its jacket and immersed in glycerin, thus forming a mode stripper ($n_{cl} = 1.458$, $n_{glycerin} = 1.473$).[75]

This fiber was then mated to a second fiber of 250 meters in length through the connecting apparatus shown in Figure 25. The driving fiber could have been excited directly by the laser, thus eliminating this connection. The intent of using the 40 meter length of fiber with the cladding mode stripper to excite the driving fiber, was to further simulate actual operating conditions. This connection again excited cladding modes but this time more representative of those found in communications cables. The connecting apparatus used two glass microscope slides to form a precision "V" groove. By placing one slide on top of another, but staggered a quarter inch, as shown in the figure, the "V" groove was formed. The junction was then made by pushing the two fibers along the groove from opposite ends, and the flex tension, caused by the angle at which the fibers were presented to the groove, held them in the groove. This was an adaptation of an idea presented by Gordon, Rawson, and Norton, but makes use of more readily available material.[76]

Another mode stripper was placed in the second fiber about a meter from its end. This time the stripper was only 13 inches in length, because it was found that longer lengths were not any more effective.[81]

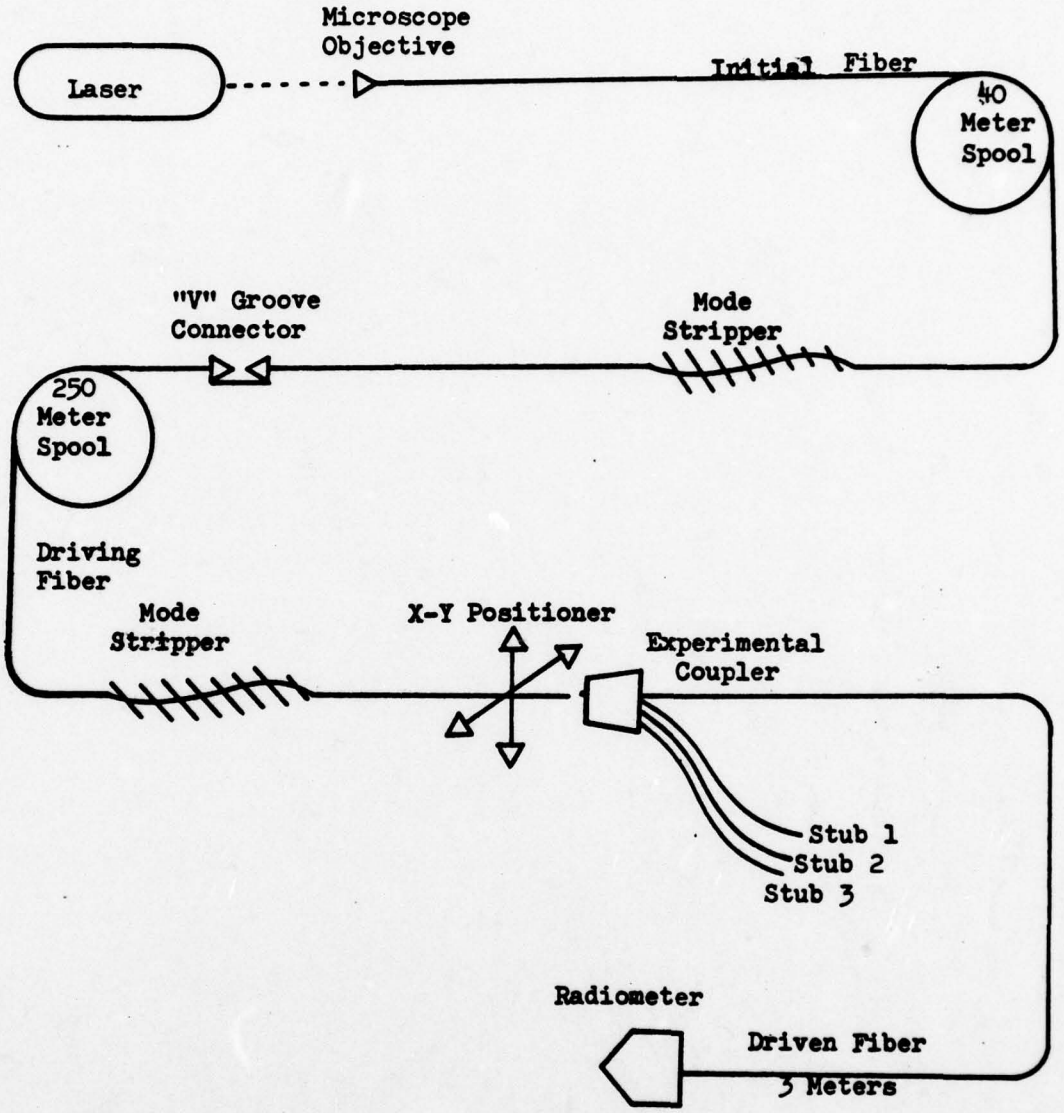

Figure 24. Schematic diagram of the experimental apparatus.

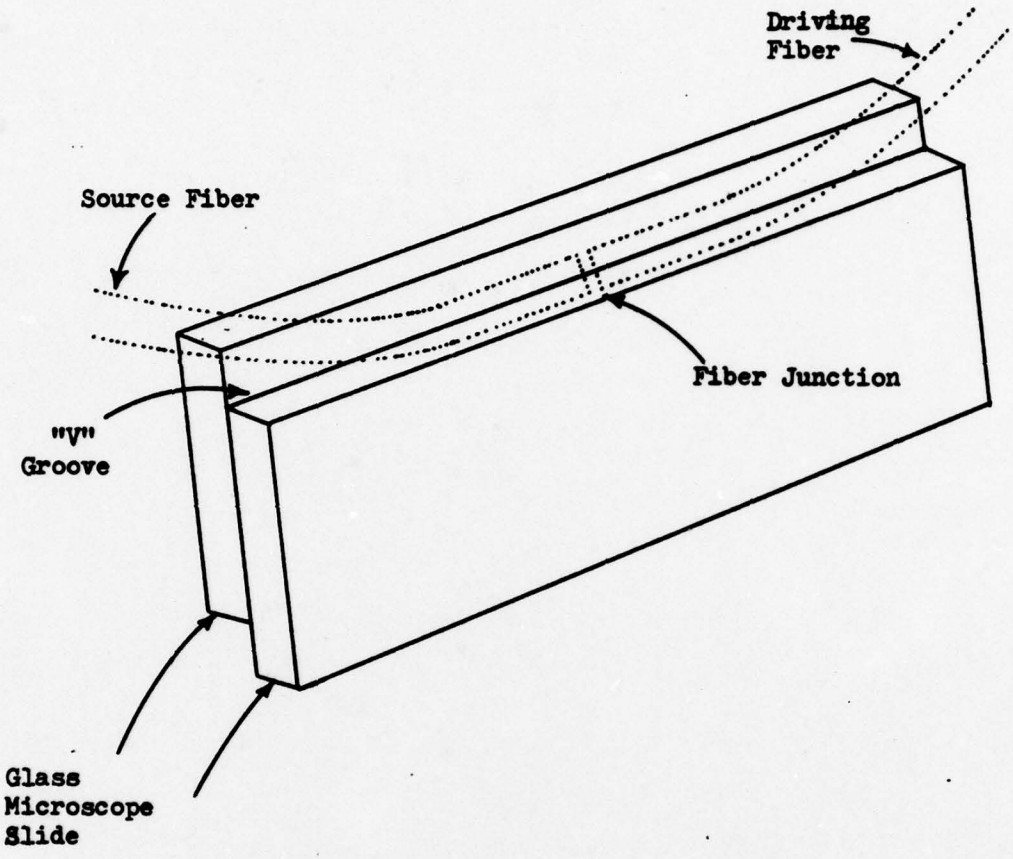

Figure 25. "V" Groove connecting device.

The second fiber (driving fiber) was terminated in an X-Y positioner. The third fiber (driven fiber) was then held in the coupler fixture (Figure 26) and mated to the second fiber in the positioner. The third fiber was three meters long and was terminated in a radiometer. Another radiometer was used to measure power in each stub individually.

All three fibers were ITT graded index, with a diameter of 125 microns, but were purchased at different times over a period of a few years. The driving fiber was the newest and the 40 meter length was the oldest. It is suspected that the 250 meter length had less dimensional variations than the 40 meter length.

The construction of the coupling fixture was started by first preparing the stub fibers. A plastic unclad fiber, with a diameter of 30 mils was chosen. The 30 mil diameter was the closest available diameter to the required diameter:

$$125 \text{ microns} \times 6.46 \div 25.4 \text{ microns/mil} = 31.8 \text{ mils}$$

Using a scalpel blade, three lengths of 16 inches each were cut from the plastic fiber. The ends of this fiber were polished using a polishing wheel at a fast speed and a Linde B abrasive, and the finished ends were examined under a microscope. To hold the fibers perpendicular to the polishing wheel a fixture was fashioned which enabled better alignment (See Figure 27). The driven fiber was cleaved on both ends by the method described in section II. The same procedure was used to prepare the ends of each glass fiber, and the ends were inspected under a microscope before being accepted.

One end of each of the three stubs was then placed in position so that the three ends formed a three rod bundle. An end of the glass fiber was introduced into the bundle interstice. Ideally, the four fibers should have been "butted" so that each of their end faces were contained in one plane, perpendicular to each of their

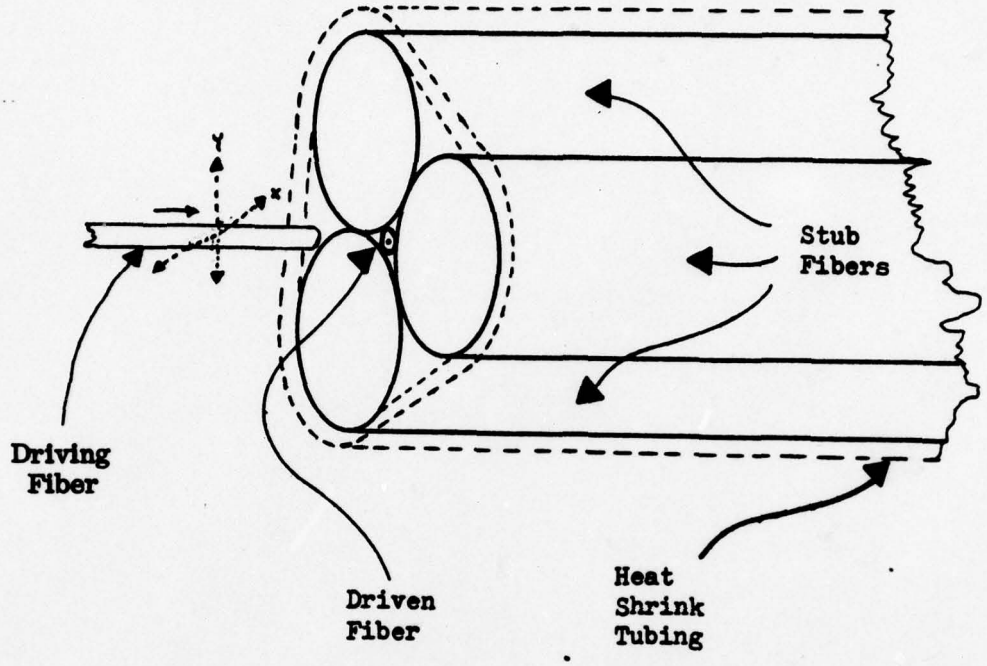

Figure 26. Experimental fiber coupling fixture.

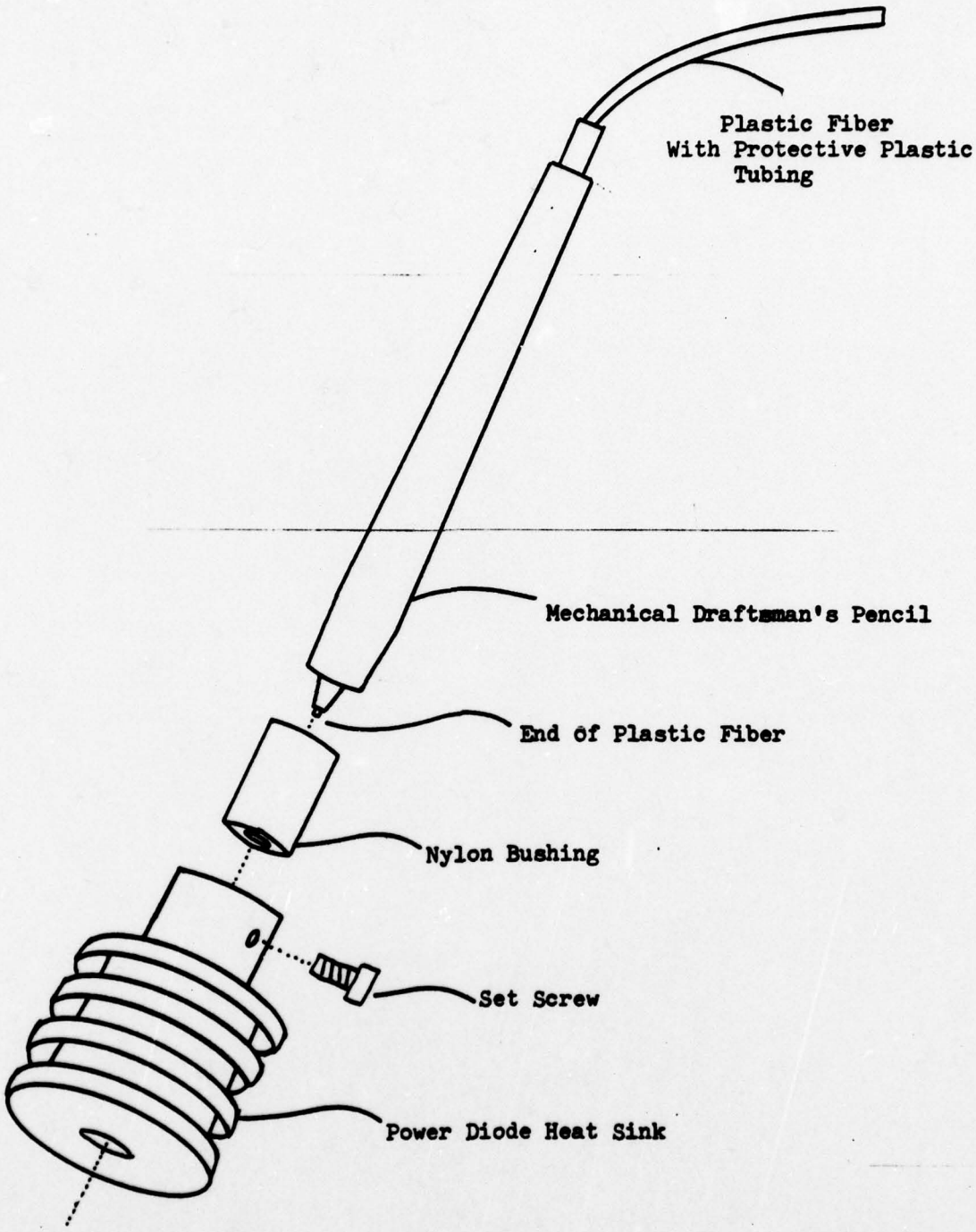

Figure 27. Plastic fiber polishing fixture.

longitudinal axes (See Figures 11 and 26). Actually, it was necessary to let the driven fiber protrude in front of the coupler face by a few mils so that its location could be distinguished from the side through a microscope. This was for measurement purposes only and would not be required in practical applications.

The bundle was then inserted into a piece of heat shrink tubing and heated to hold the bundle together. The coupling length was limited to three centimeters by the fact that the nylon jacket on the driven fiber was only stripped back to three centimeters from the fiber end. It was important not to use too much heat in shrinking the tubing, because the plastic fiber melts at about the same temperature that shrinks the heat shrink tubing.

The completed fiber bundle was then inserted into a lead holder similar to the one used in the polishing fixture. The coupler was then fastened to the X-Y positioner in a way that the driving fiber could be mated precisely to the driven fiber and could be offset in two orthogonal directions (X and Y). The positioners used during this experiment were ordinary micrometer barrels, with a smallest division of one mil. Each mil was visually divided into five divisions of approximately five microns each, and it was felt that each position could be estimated to within -1.5 microns. This gave each position an uncertainty of approximately 3 microns. To improve the experimental error, differential micrometers, with a resolution of one micron should be used.

The experiment was started by optimizing the input to the 40 meter length of fiber. The focused laser beam was first centered on the fiber, then the longitudinal axis of the end of the fiber was made parallel to the axis of the light beam. The beam was then centered again and the separation between the microscope objective and the fiber face was adjusted. While monitoring the power at the end of the fiber, the launching position of the fiber was adjusted until peak power was

found.

The next task was to optimize the splice between the 40 meter fiber and the 250 meter fiber. The connection was observed under a microscope. Alcohol was used to wash any dirt from between the two fibers. The alcohol was then allowed to evaporate and a drop of glycerin was inserted between the two fiber faces as they were pushed together. In the future it would be advantageous to place a metal cylinder in the groove over the two fibers to help hold them in place. The geometry of this relation is shown in Figure 28.

The opposite end of the 250 meter fiber was fastened in the translatable side of the X-Y positioner, where it was adjusted to zero offset in relation to the driven fiber in the coupler fixture. When adjusting it was viewed under the microscope, along both the X and Y axes to assure zero offset. Then the end separation was set to about 5 microns to avoid abrasion between the two fiber faces. The output end of the driven fiber was always terminated in a radiometer. One of the stubs was also terminated in a radiometer. The fiber face was oriented to the X-Y axes as depicted in Figure 29.

The actual experimental procedure was started by initializing the coupler and terminating stub number one in the radiometer. The driving fiber was translated first in the positive Y direction, and the power was recorded for the driven fiber and for stub number one at intervals of five microns displacement. Although a large range was recorded, it was found that the micromanipulators did not give accurate displacements after about 70 microns from the center. This displacement was quite adequate for the project at hand.

The coupler was again initialized and data was collected along the negative Y direction. This data is recorded at Figure 30. Power fluctuations plagued the experiment throughout its progress. The largest power fluctuation observed in the

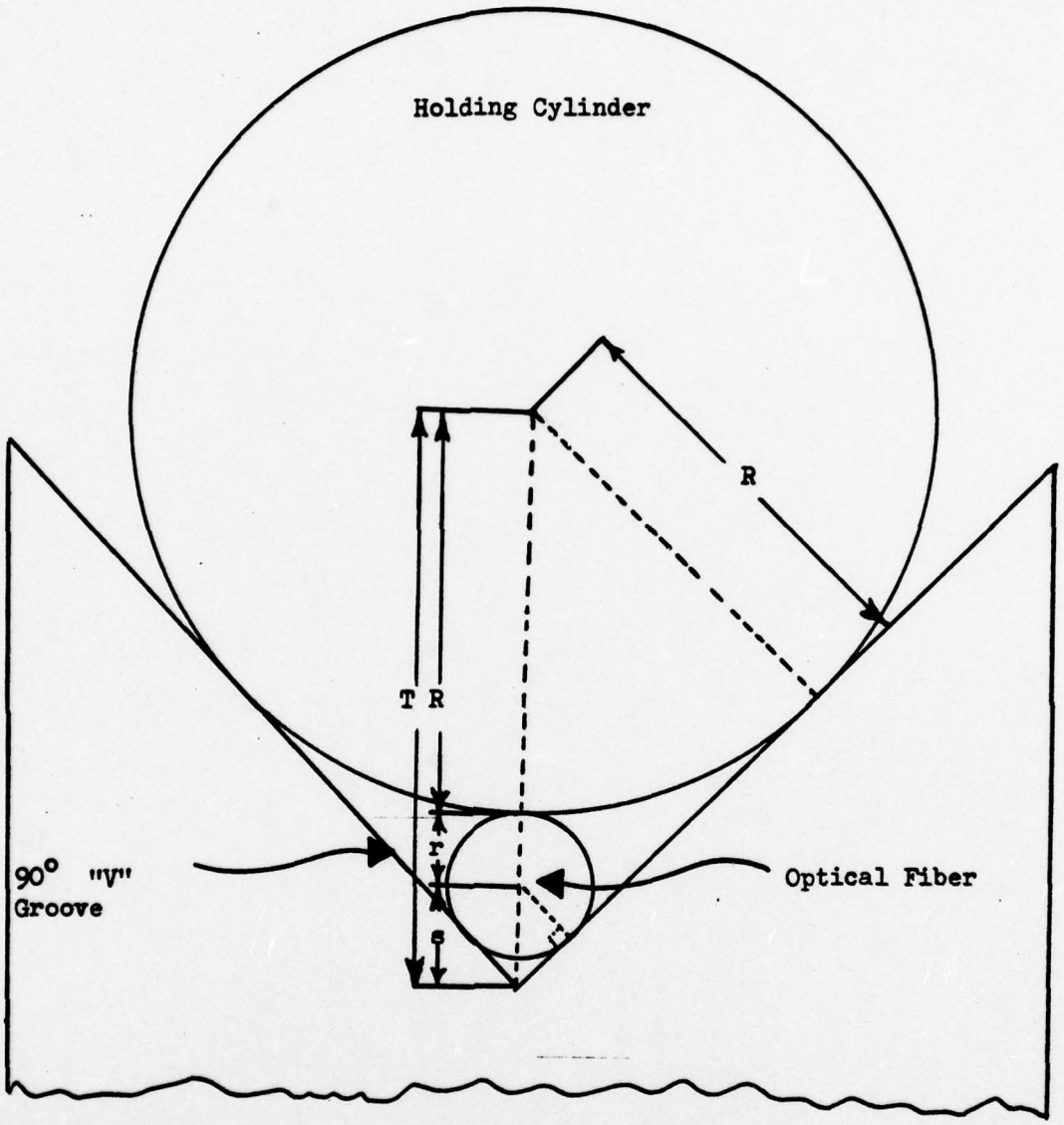

$T = R + r + s$

$R = T \sin 45^\circ$

$R = 5.83\ r$

Figure 28. "V" Groove holding rod geometry.

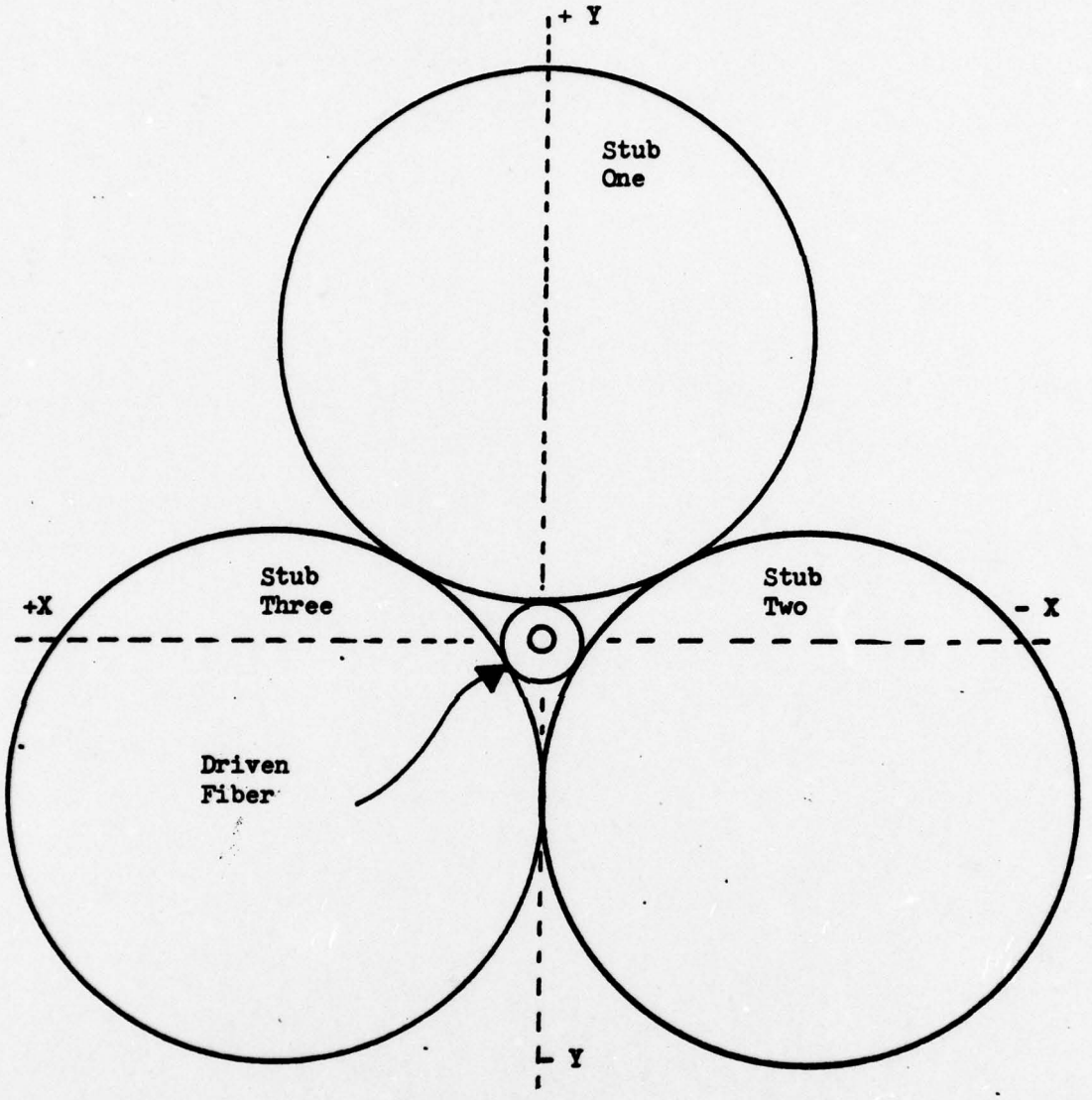

Figure 29. Orientation of X and Y axes of the coupler face.

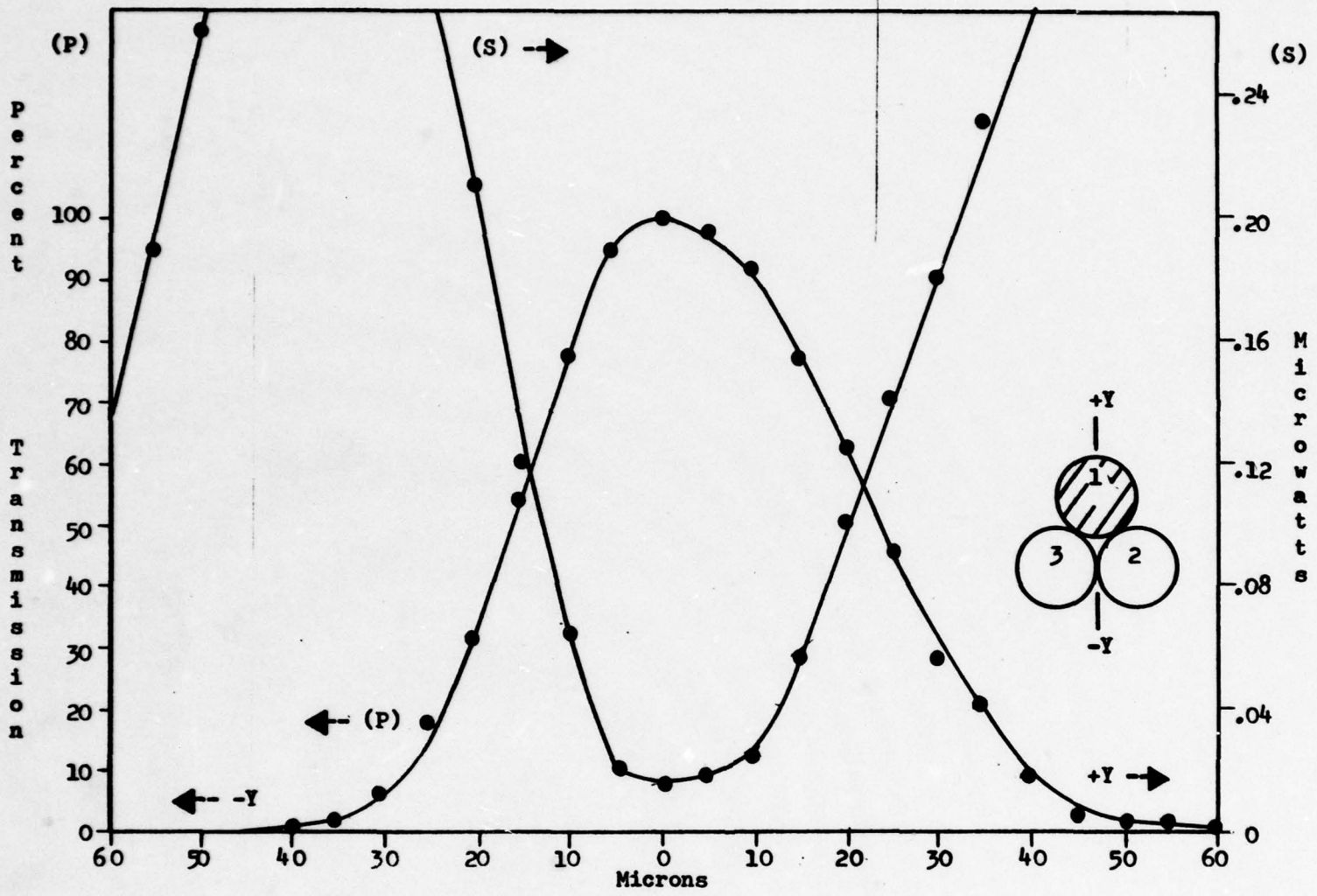

Figure 30. Percent power transfered through the connection vs. offset in the "Y" direction. (P) Power coupled to stub fiber number one vs. offset. (S)

driven fiber as a result of source fluctuation was 20 microwatts, which is five percent of the 390 microwatts measured in the driven fiber at zero offset. The adverse effect of the power fluctuations was reduced satisfactorily by recording the driven fiber power after it was normalized by its peak value at zero offset. This did not eliminate the small quick changes in source power level, but it did reduce the effects of the larger more gradual power shifts.

The coupler was again initialized, translated in the positive X direction, and then the procedure repeated in the negative X direction. This data is shown in Figure 31. The same data (all four radials) was recorded for stubs two and three and is shown in Figures 32 - 35.

Note the deformity in the stub power curve of Figure 34. The reason for this departure from the other data is not fully understood. This problem did not occur in subsequent runs and could not be duplicated. It is felt that the stub came loose from the radiometer during that run. Figure 34 also shows that even under adverse conditions the lowest stub power still occured at zero offset.

The coupler face was rotated at 30^{o} intervals from -30^{o} to 60^{o}. The power versus offset data were recorded for the Y axis at each interval of coupler rotation. This was performed to determine if the stub power was indeed independent of the angular orientation of the radial displacement. Figures 36 - 39 show that the stub power displayed the same general relation for each radial for offsets below 37.5 microns.

Figure 40 illustrated a run that was made with all three stubs in the radiometer. After the stub power scale was multiplied by three, this figure assumed the same shape as the others.

Finally the stubs were each terminated in a holding fixture which held their ends in the same orientation as they appeared on the coupler face (See Figure 41).

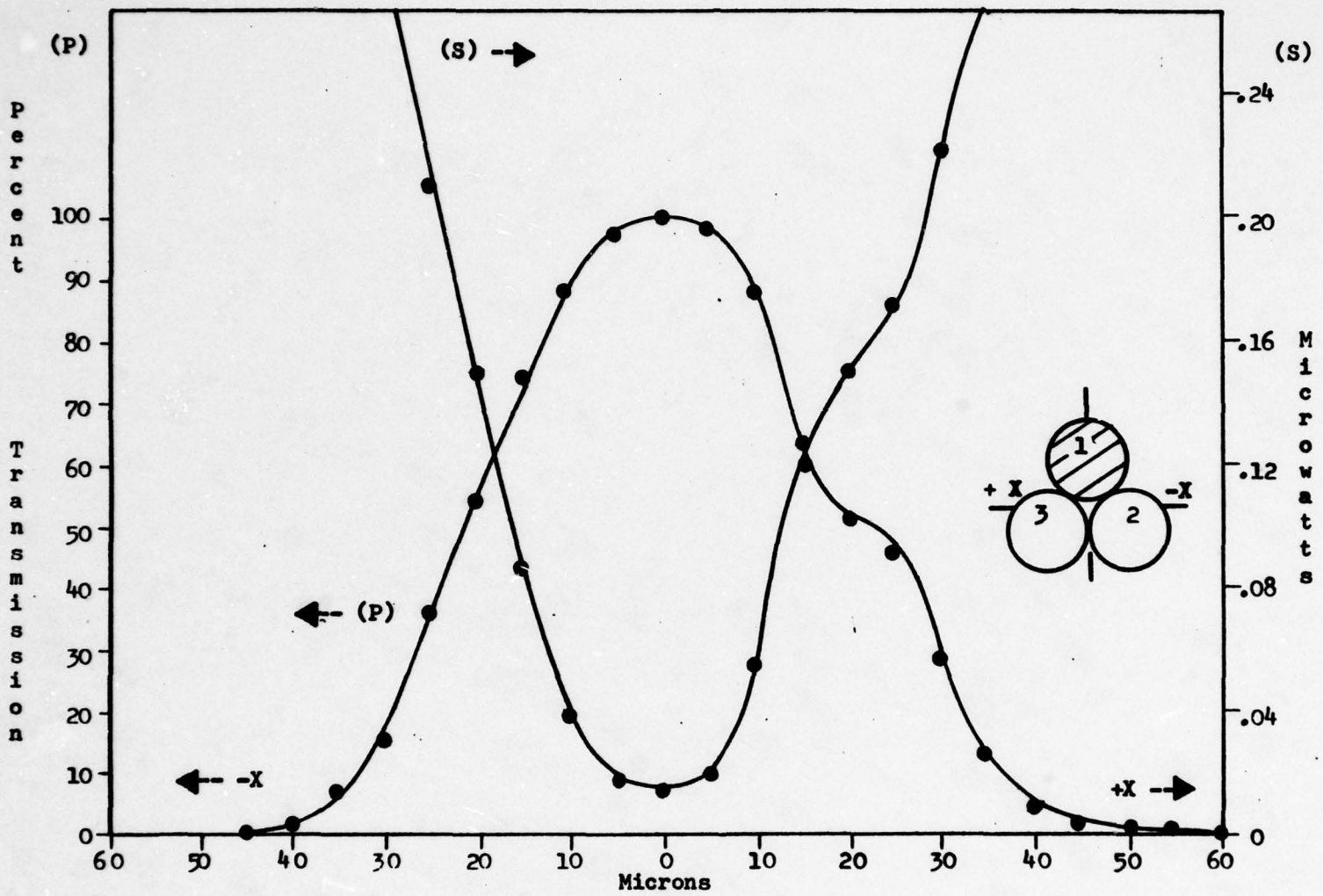

Figure 31. Percent power transferred through the connection vs. offset in the "X" direction. (P) Power coupled to stub fiber number one vs. offset. (S)

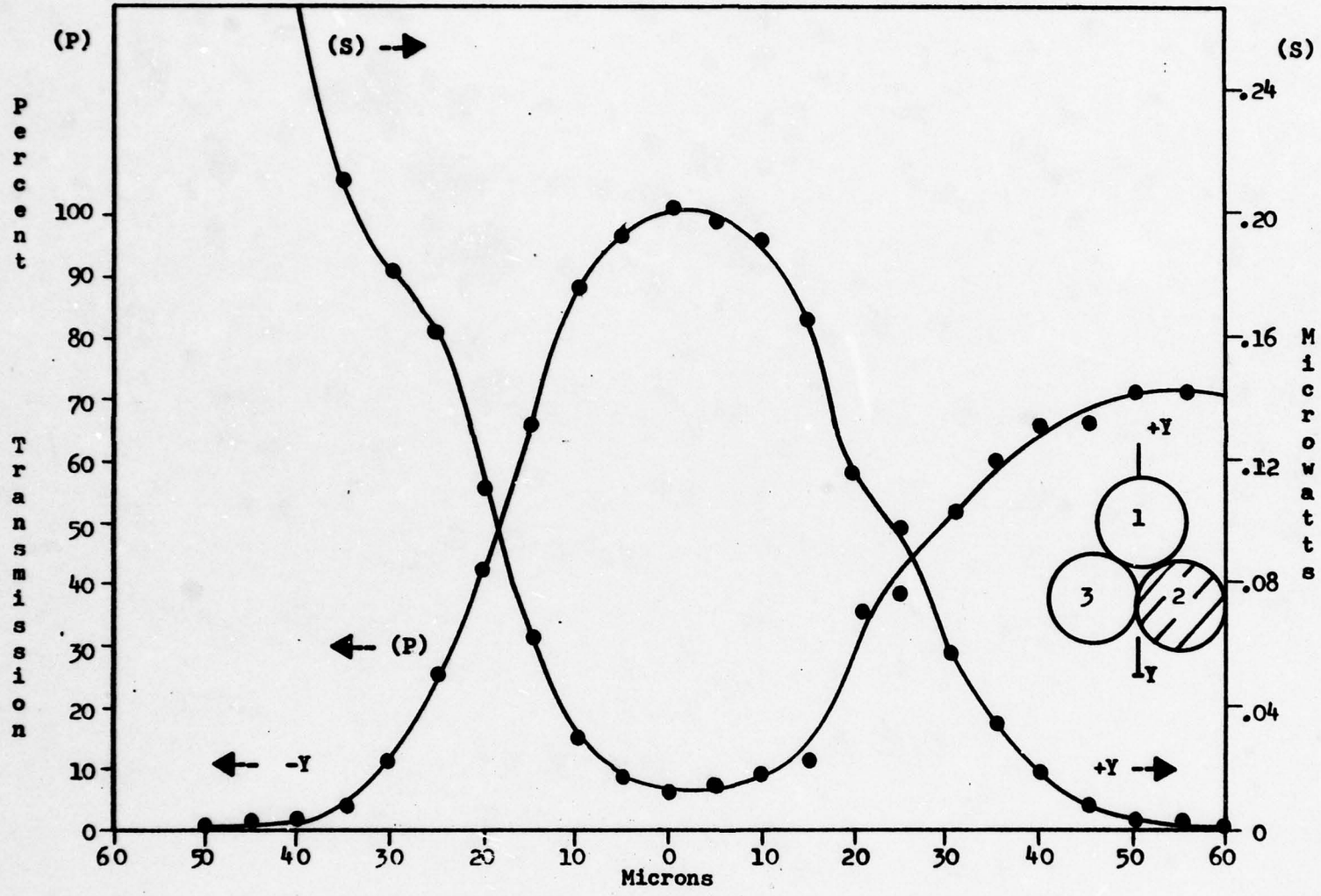

Figure 32. Percent power transfered through the connection vs. offset in the "Y" direction. (P) Power coupled to stub number two vs. offset. (S)

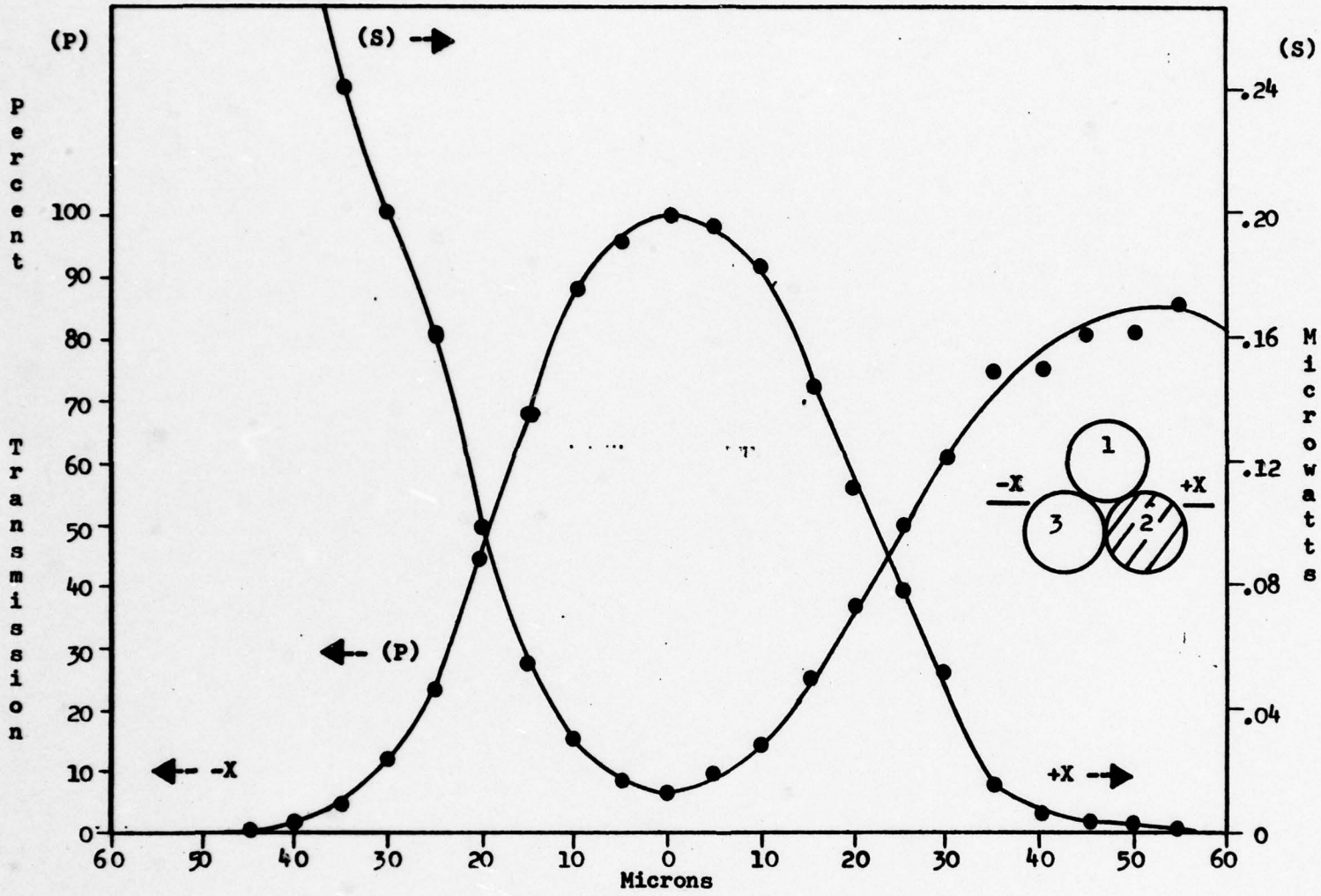

Figure 33. Percent power transfered through the connection vs. offset in the "X" direction. (P) Power coupled to stub fiber number two vs. offset. (S)

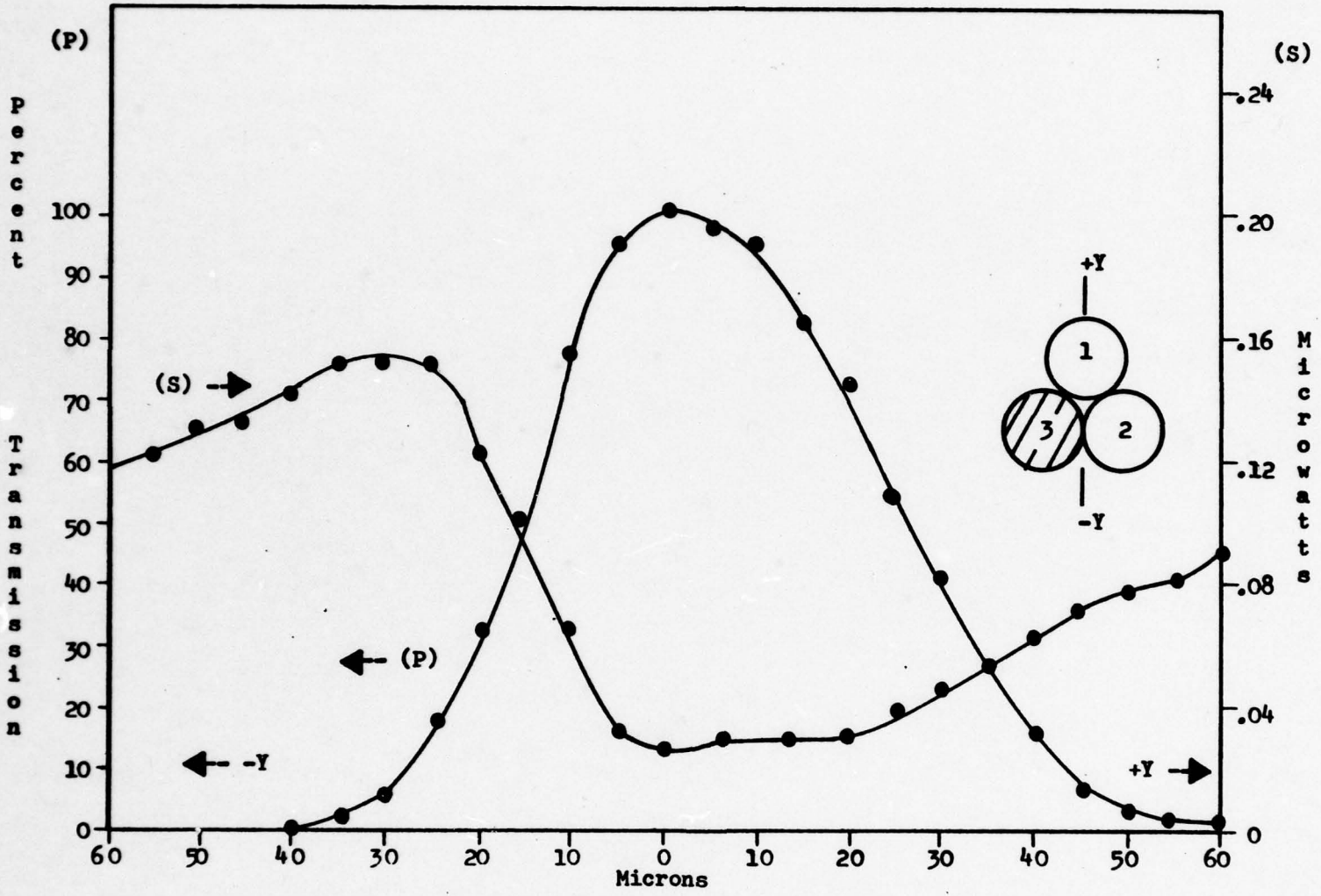

Figure 34. Percent power transfered through the connection vs. offset in the "Y" direction. (P) Power coupled to stub number three vs. offset. (S)

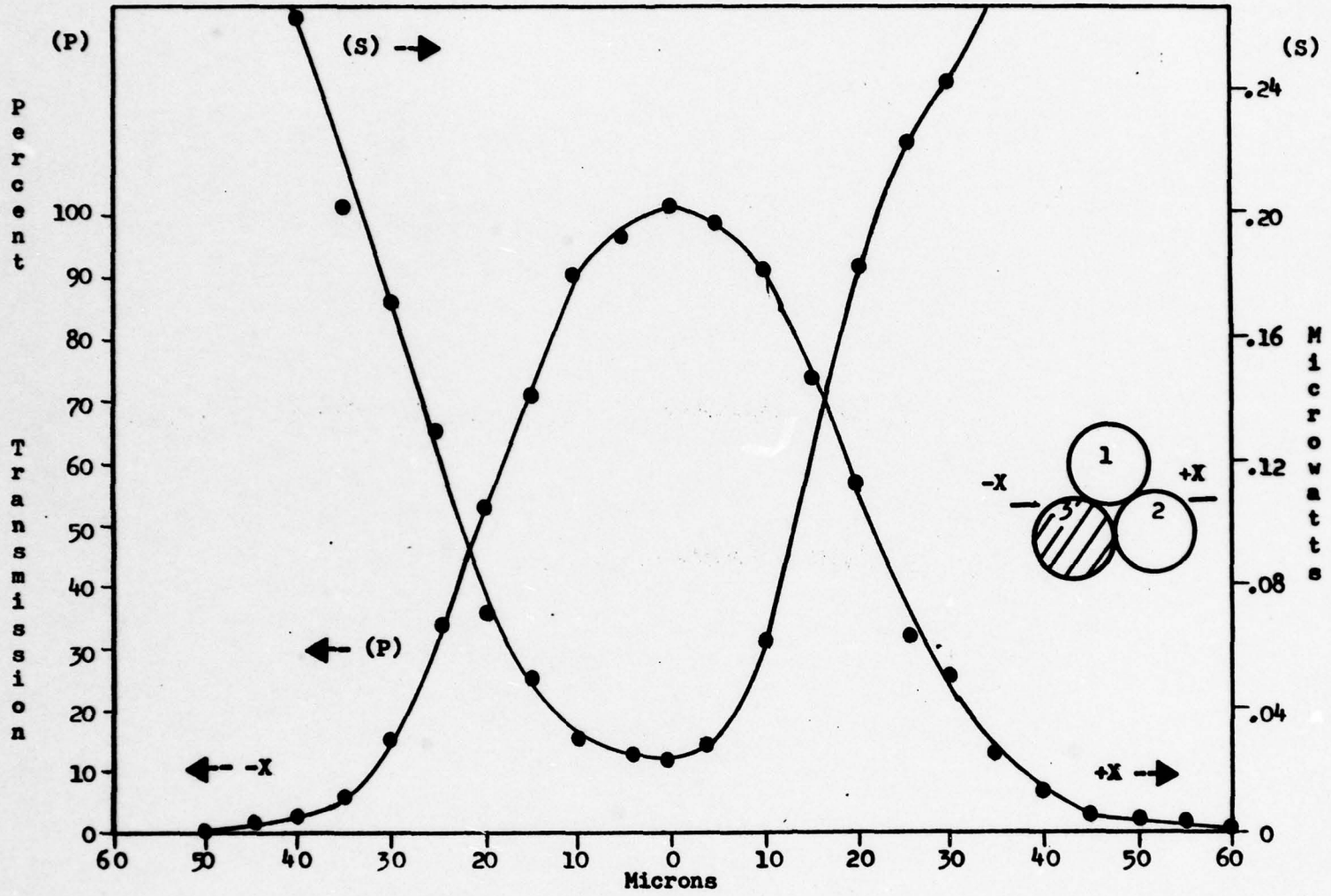

Figure 35. Percent power transfered through the connection vs. offset in the "X" direction. (P) Power coupled to stub number three vs. offset. (S)

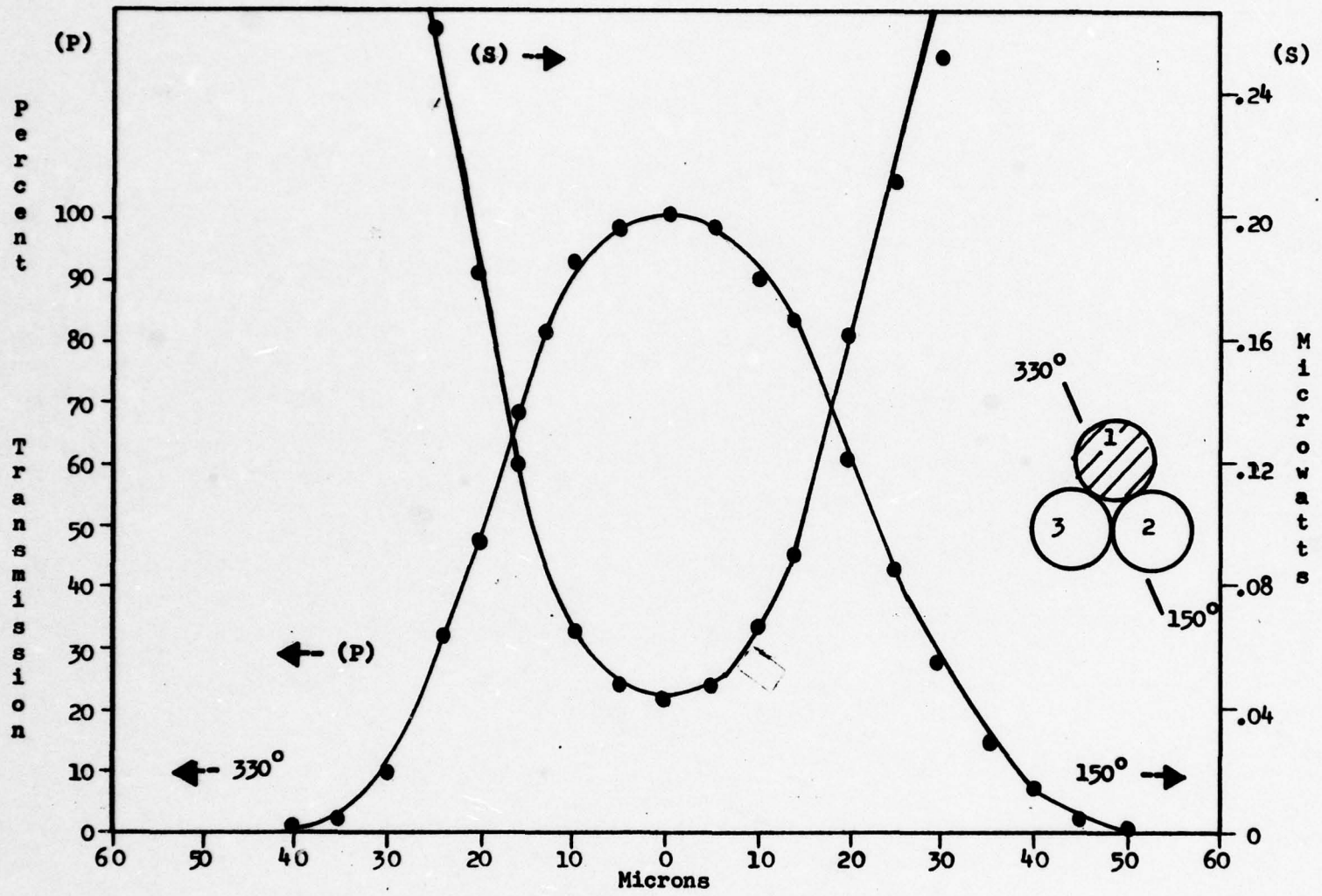

Figure 36. Percent power transfered through the connection vs. offset for the 330° and 150° radials. (P) Power coupled to stub number one vs. offset. (S)

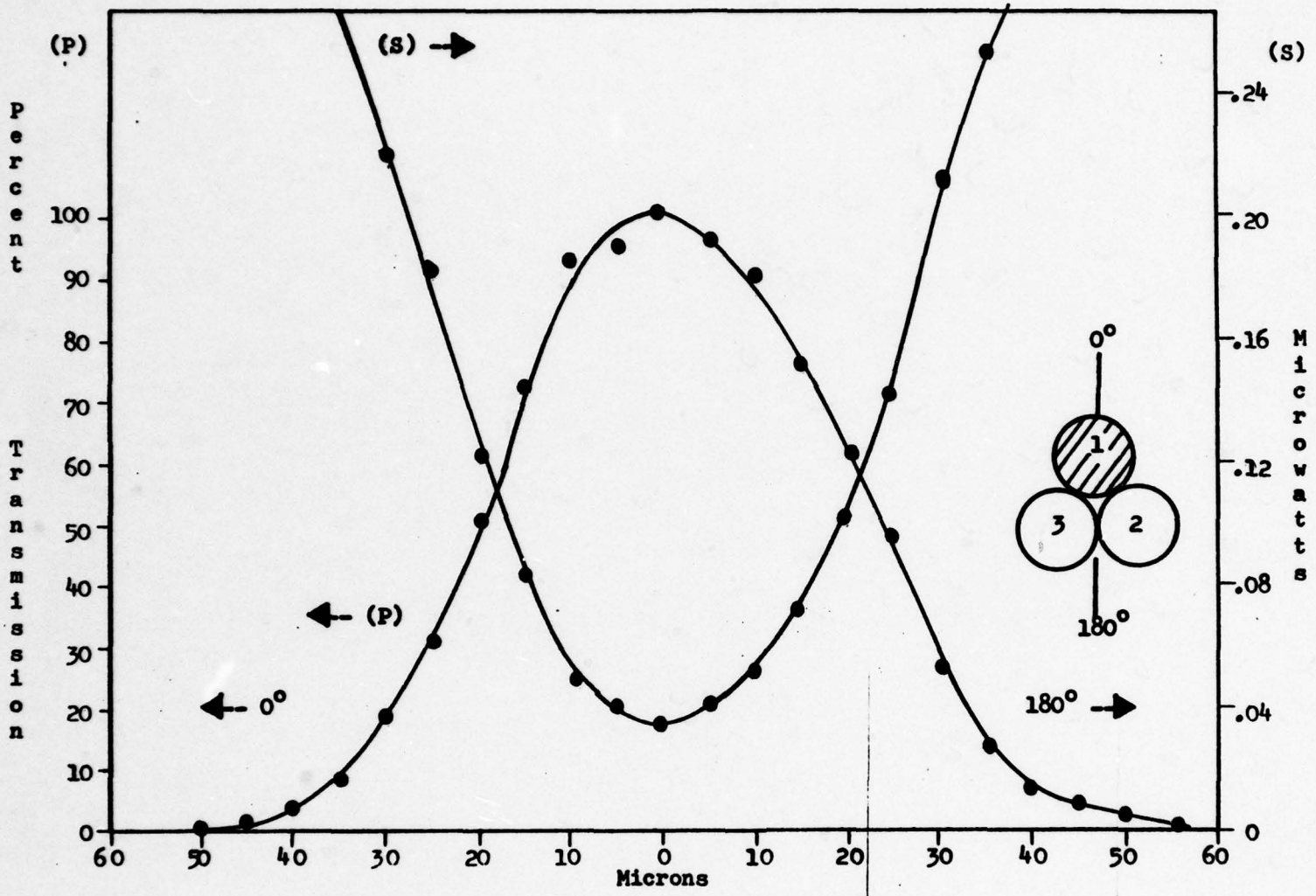

Figure 37. Percent power transfered through the connection vs. offset for the 0° and 180° radials. (P) Power coupled to stub number one vs. offset. (S)

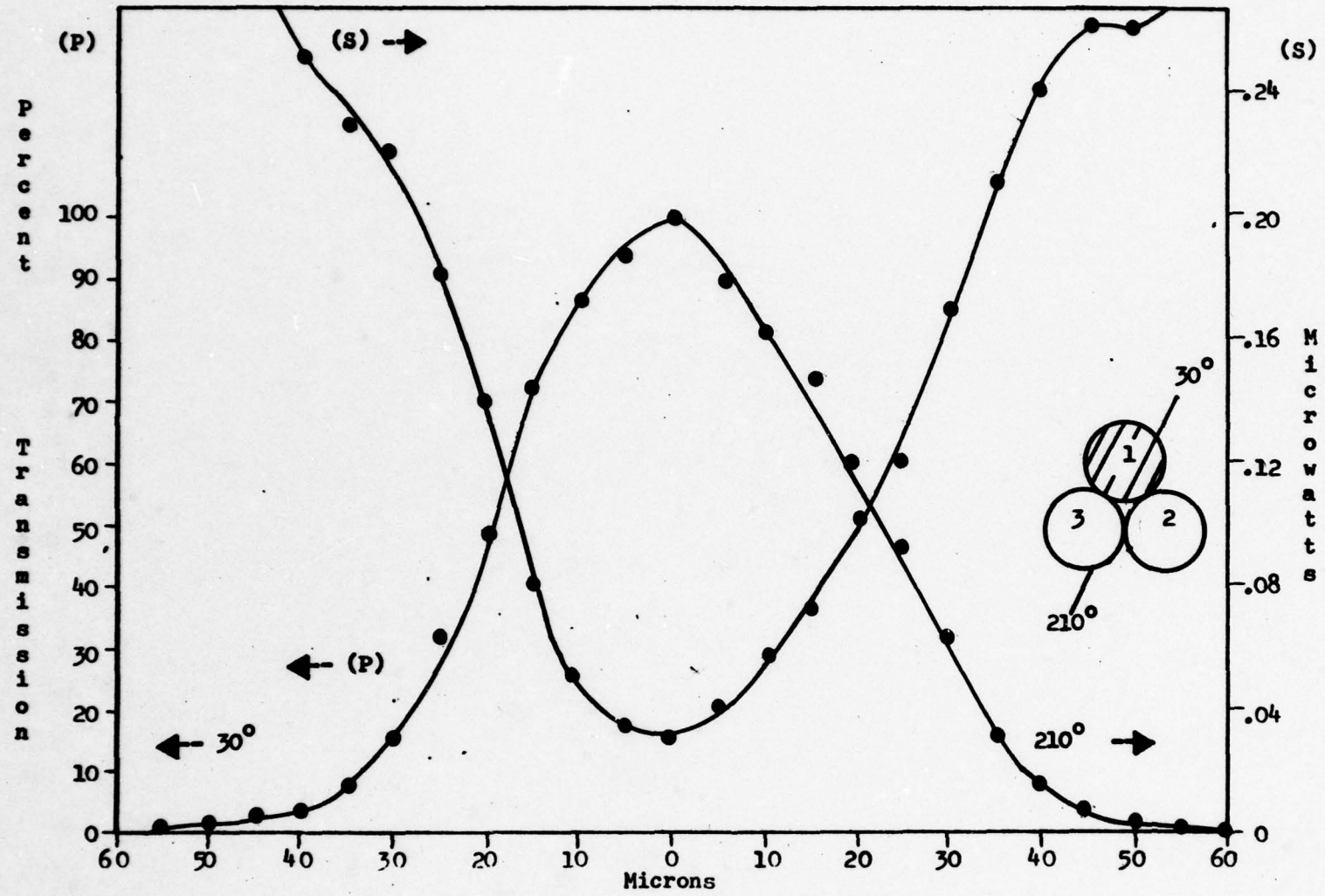

Figure 38. Percent power transfered through the connection vs. offset for the 30° and 210° radials. (P) Power coupled to stub number one vs. offset. (S)

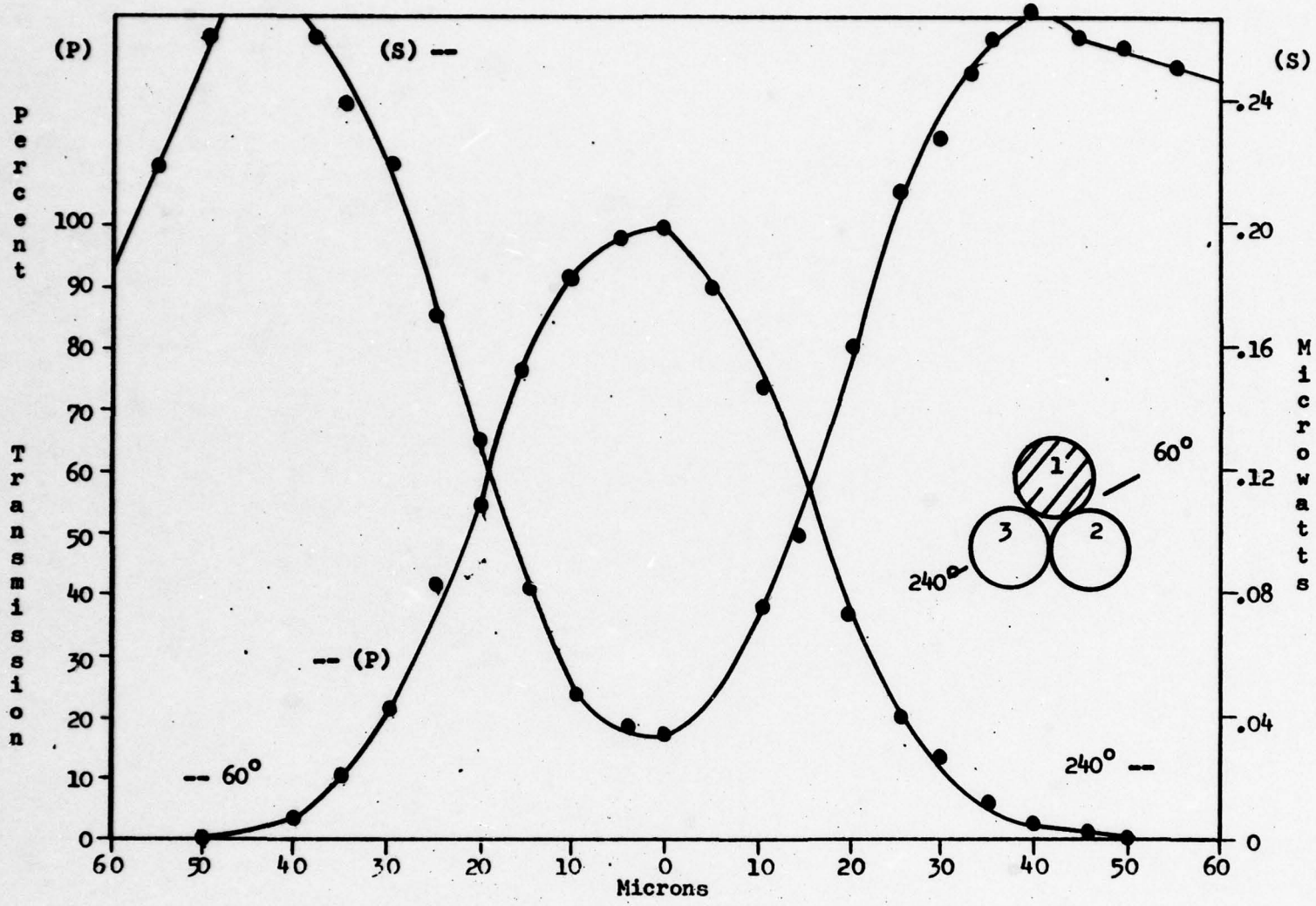

Figure 39. Percent power transfered through the connection vs. offset for the 60° and 240° radials. (P) Power coupled to stub number one vs. offset. (S)

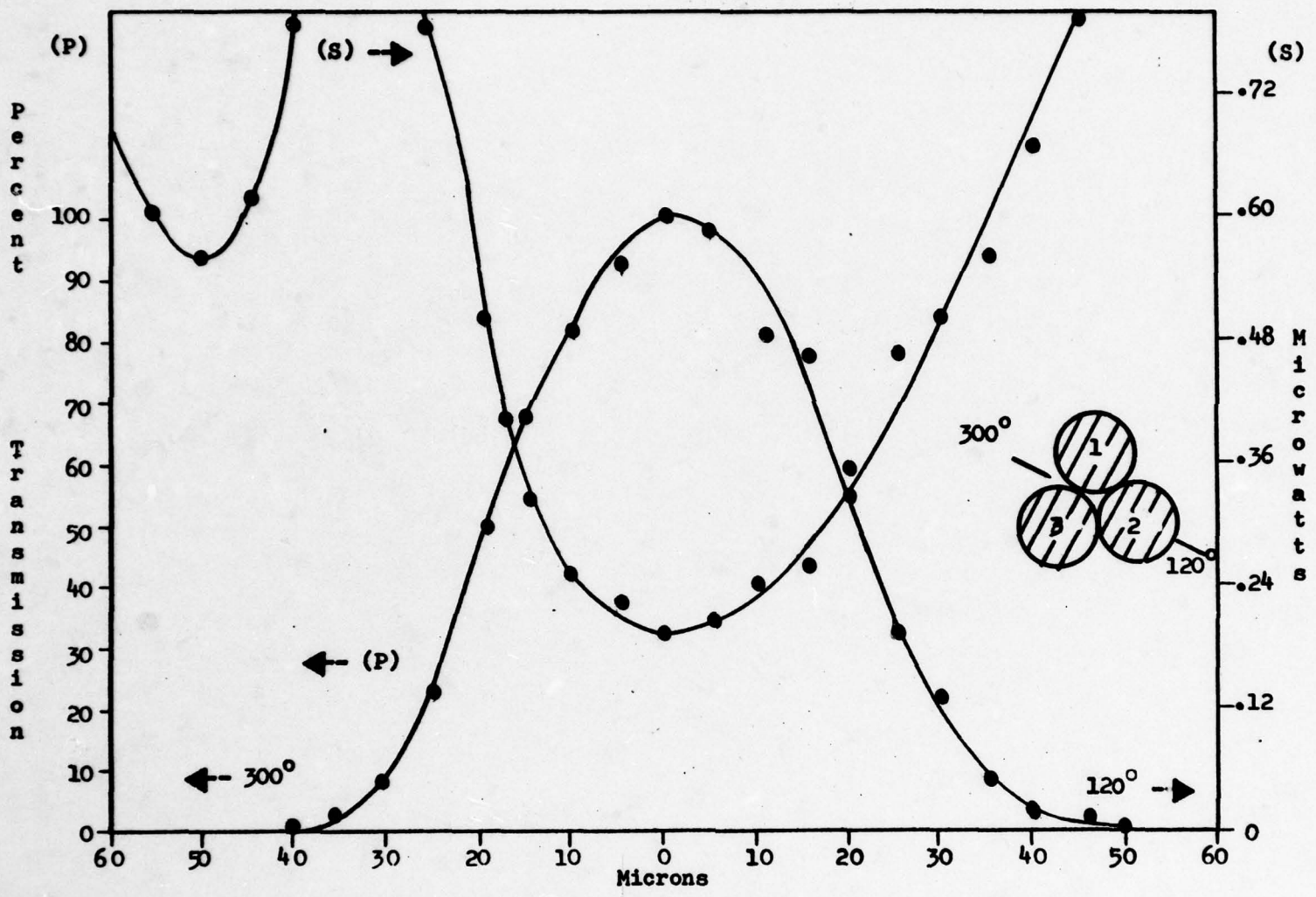

Figure 40. Percent power transfered through the connection vs. offset for the 120° and 300° radials. (P) Power coupled to stub fiber numbers one, two, and three, vs. offset. (S)

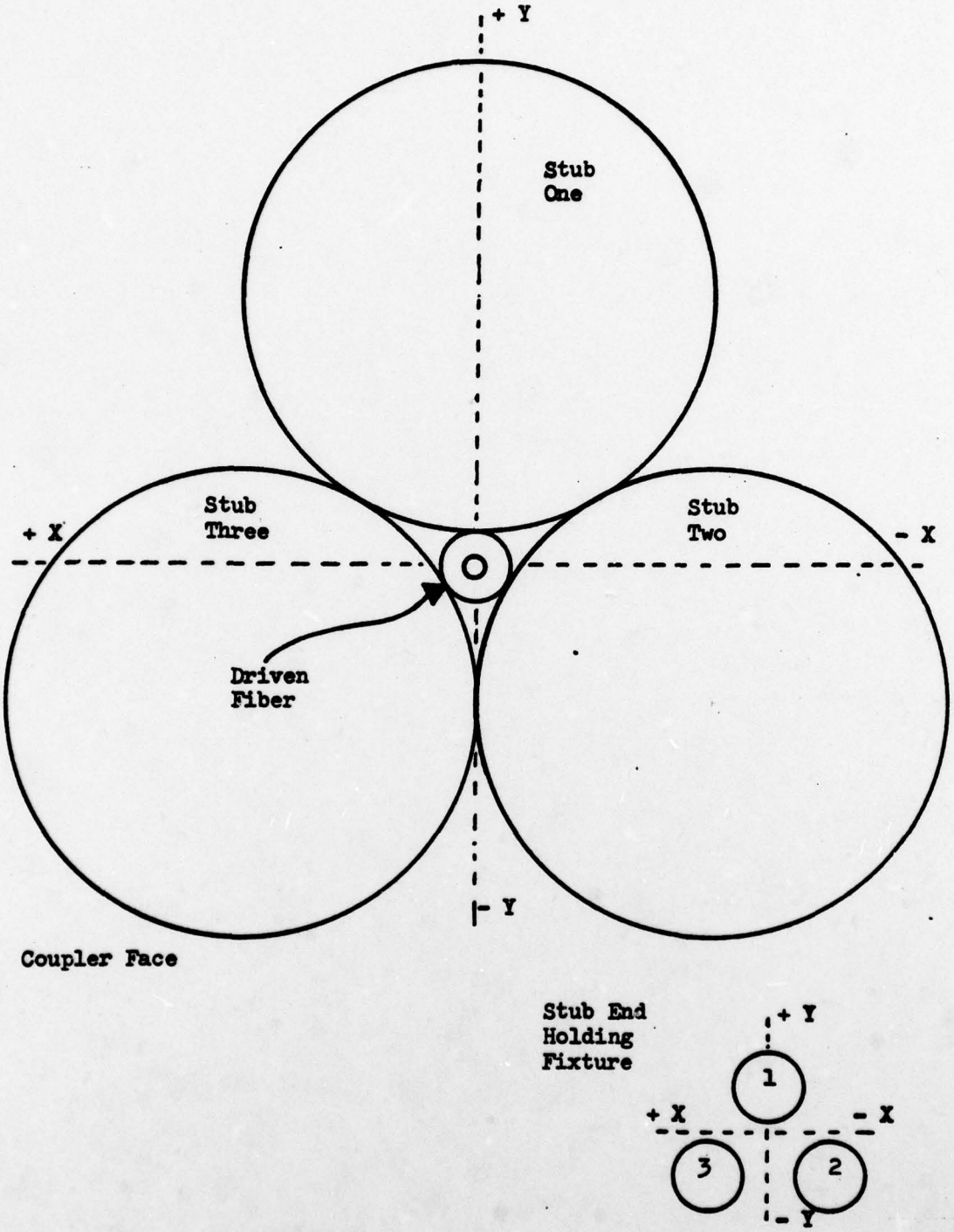

Figure 41. Comparison between cordinate systems for fiber coupler face and the Stub end holding fixture.

It was found that any offset could be reduced to zero just by observing the light intensities in the stubs with the unaided eye. If fiber number two was brighter than the others (See Figure 42), the positioner was moved in the -X direction until two and three were equal (See Figure 43), then the positioner was moved in the +Y direction until all three fibers showed equal intensity (See Figure 44). At this time it is important to remember that when the stubs show equal intensity, the offset is not zero, it is only within 37.5 microns of being zero. The positioners were then carefully manipulated until all intensities reached a minimum (See Figure 45). It was found that the unaided eye could detect a minimum in light intensity, as well, if not better than, by using a radiometer. After some practice, the author could align fibers by this method in less than twenty seconds on the average. The technique was taught to six different people. Each of the subjects learned the technique in less than five minutes and could align fibers in less than one minute.

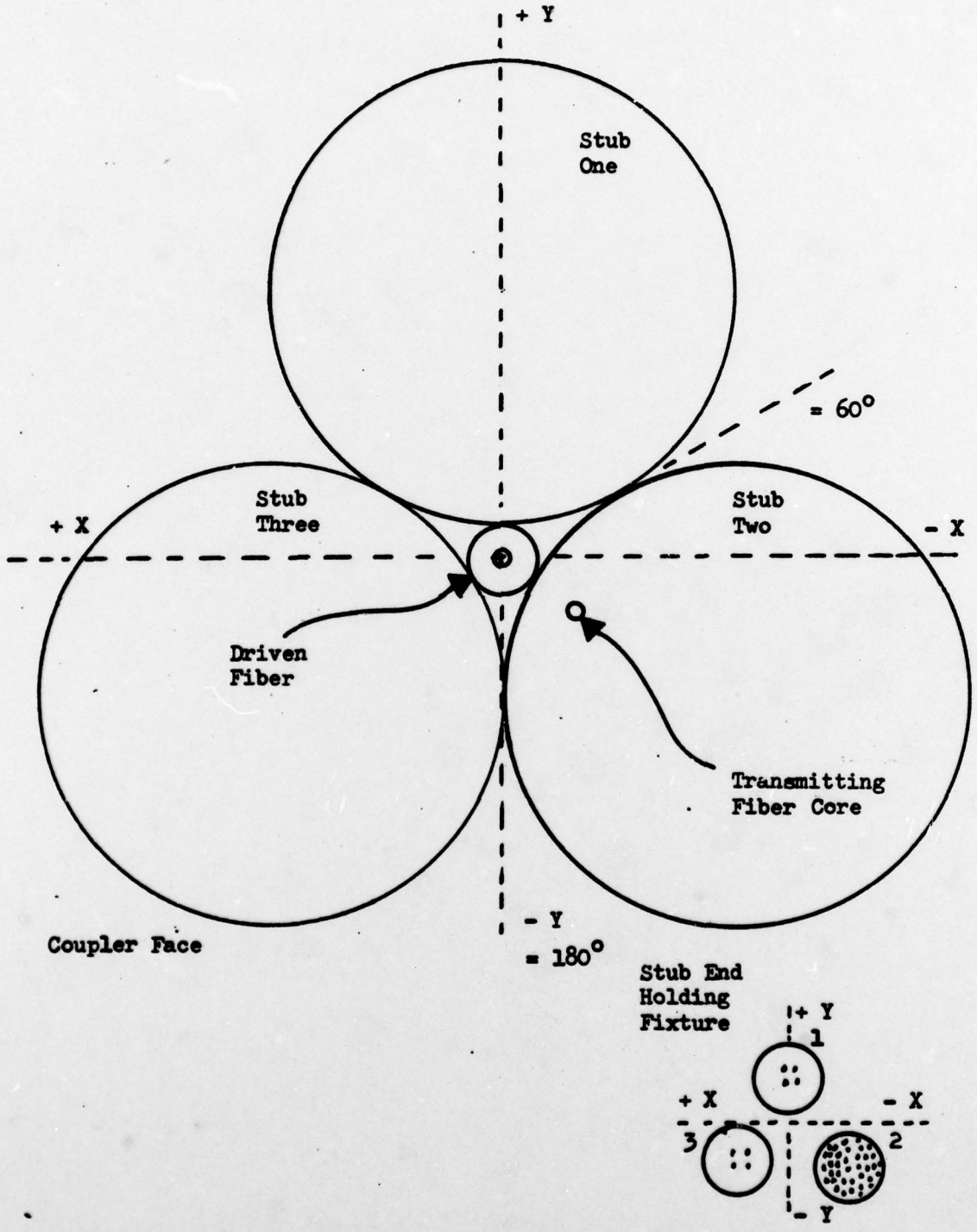

Figure 42. The offset transmitting fiber core located somewhere in the section of the coupler face bound by the = 60° and = 180° radials. The relative light intensity is represented by the number of dots in the circle representing a given fiber end.

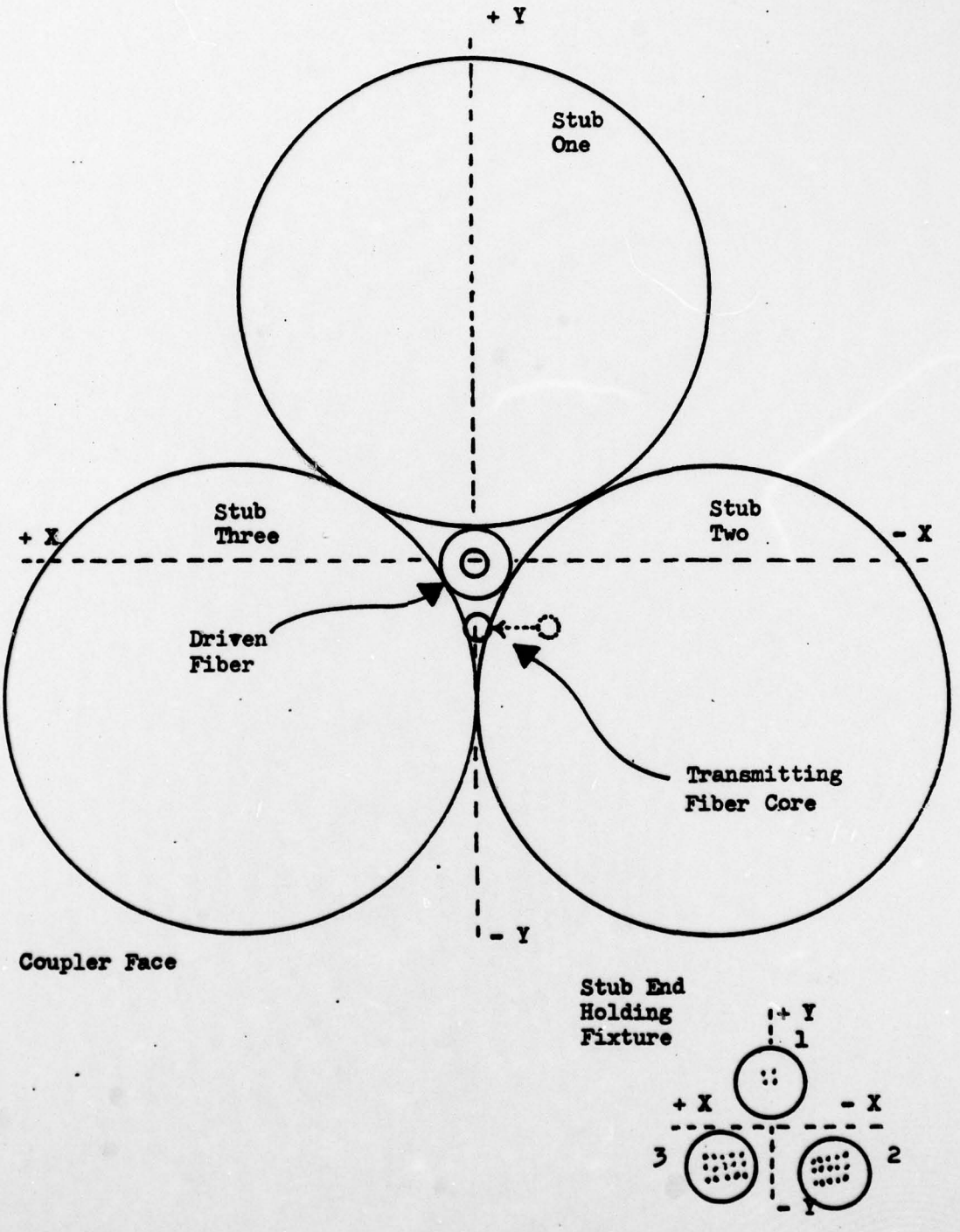

Figure 43. The offset transmitting fiber core translated in the negative X direction. The relative light intensity is represented by the number of dots in the circle representing a given fiber end.

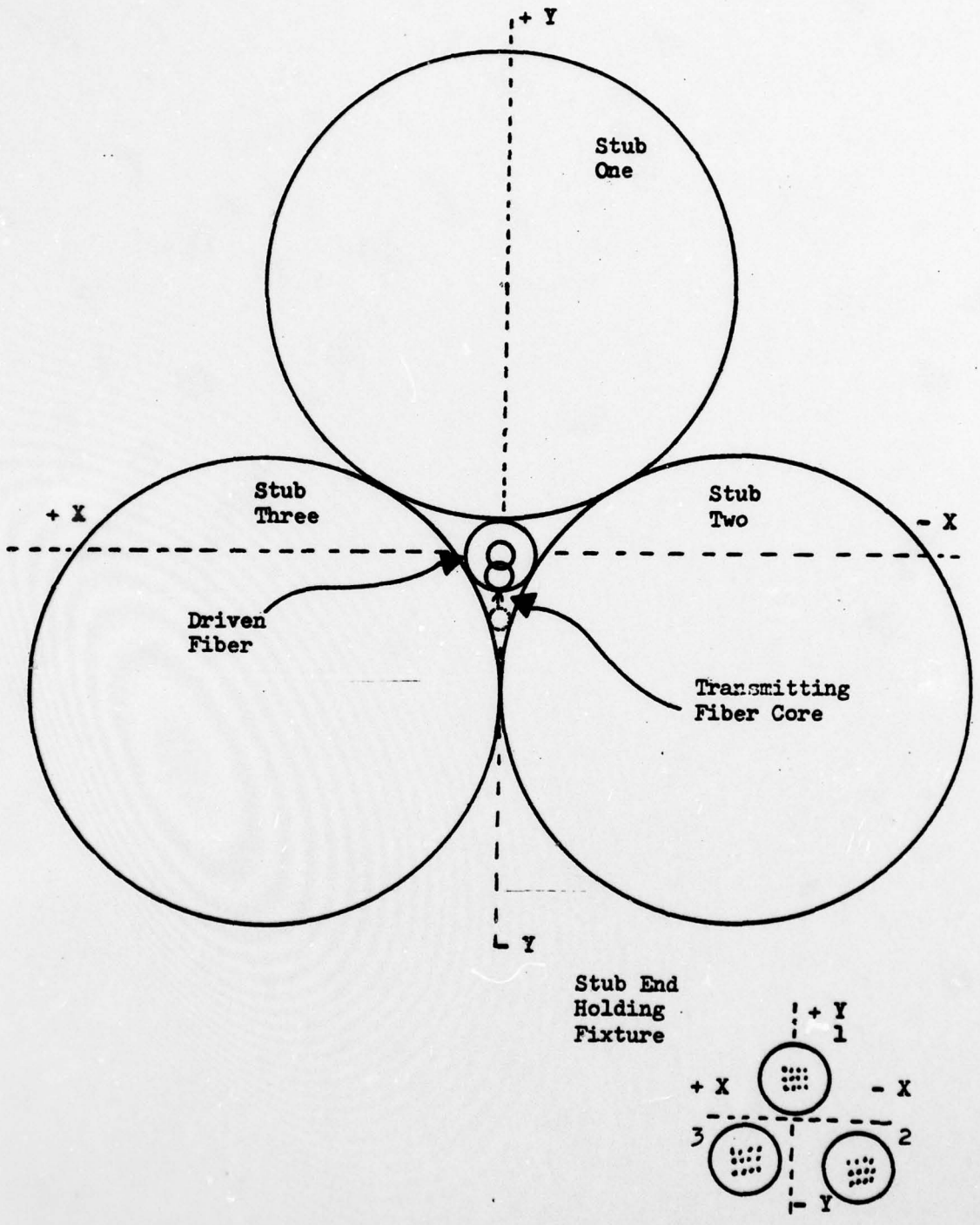

Figure 44. The offset transmitting fiber core translated to within the cladding circumference of the receiving fiber. The relative light intensity is represented by the number of dots in the circle representing a given fiber end.

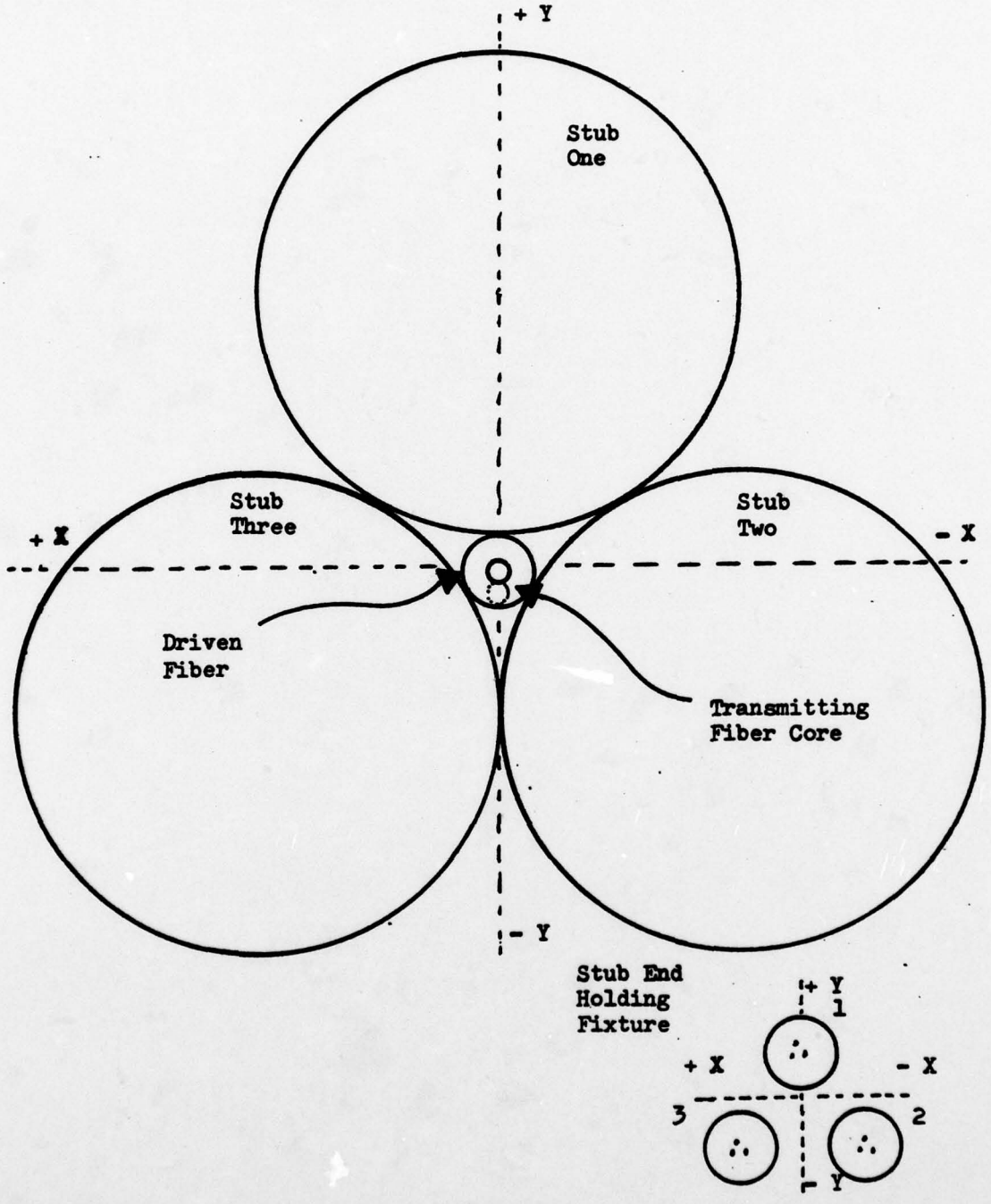

Figure 45. The transmitting fiber core adjusted to zero offset. The relative light intensity is represented by the number of dots in the circle representing a given fiber end.

VII. DISCUSSION OF RESULTS

The stub power vs. displacement curves in section V all show the same shape for displacement values less than 37.5 microns. This agrees with the second theoretically predicted trend listed at the end of section V. It also supports the assumption made in that section, that light entering the receiving fiber at any point on the face of the receiving fiber will, within a very short propagation distance, assume a power distribution which is independent of the angular component of the radius vector to the point of entry.

The calculated power transfer between fibers (See Figure 20) resembles the measured curves in section VI. The measured values (See Figures 34 - 44) were not measured under the ideal conditions which were assumed for the theoretical calculations. End separation and tilt were not eliminated and could not be maintained constant between data runs, so the curves vary to some degree from one to another. This was caused by the limitations of the apparatus. However, the shapes of the curves coincided, showing that general trends of increasing and decreasing power could be reasonably approximated by the calculated relation of Figure 20.

The "eyeball" method, described at the end of section VI was used to first detect the general dislocation and then to minimize the intensity of light from the end of the stub fibers. This confirmed the first theoretical finding of section V, which said that, for radial displacements greater than 37.5 microns, the relative position on the coupler face can be identified by the differing power levels of the stubs.

The third predicted trend of section V was that the power in the stubs all decreased to zero as the radial displacement decreased to zero. This prediction

was again made for idealized conditions of zero tilt and end separation. It was found experimentally that the power decreased to a minimum value when the radial offset decreased to zero. This indicates that loss mechanisms other than offset were present but were only evident when offset was zero. It can then be said that, under the ideal assumptions of section V, the experimental results confirm the predictions of section V.

Thus, it has been shown both theoretically and experimentally, that: 1) for radial displacements greater than 37.5 microns, the relative position on the coupler face can be identified by the differing power levels of the stubs; 2) for radial displacements less than 37.5 microns, the power levels in each of the stubs will be equal, and will vary identically for radial displacements in any direction; and 3) the power in the stubs all decrease to a minimum value as the radial displacement decreases to zero. Collectively, these findings show that the three stub coupler can indeed be used to minimize offset and maximize power through an optical fiber junction.

VIII. CONCLUSIONS

It has been shown that, using the three stub fiber coupler, the relative offset between two optical fiber waveguides can be determined. For radial displacements greater than a critical radius (37.5 microns for the fiber used in these experiments) the relative position on the coupler face can be identified by the differing power levels of the stub fibers. That is, if one stub has a higher value of power than the other two, the position of the offset transmitting fiber core is known to be located in that section of the coupler face which is bounded by the radials tangent to that stub. Likewise, if two stubs show equal intensity which is higher than that of the third, the location of the transmitting fiber core is known to be on the radial which separates those two stubs. For radial displacements less than that critical radius, the power levels in each of the stubs will be equal, and will vary identically for any displacement along any radial. It was also shown that the power in the stubs all decrease to a minimum value as the radial displacement decreases to zero and the power through the driven fiber maximized. In the above manner, it was shown that by using the three stub connector, offset misalignment at a junction between two optical fibers can be eliminated, thus maximizing the power transfer.

A very interesting aspect of this project was the "eyeball" method. This method showed that practical applications of this technique can be made which do not require expensive measuring devices. Optical communication applications usually operate in the infrared region of light, which would preclude "eyeballing" the stubs. However, materials are available which emit visible light when energized with infrared radiation. The stub ends could be coated with such a material and the "eyeball" method would again be practical.

The coupler could also be used to "tap off" a percentage of the power running

through a given fiber. The stubs would be all terminated at one detection device. This application constitutes a "Tee" coupler with the strength of the signal to be diverted at the local branch of the "Tee" being dependent upon the radial displacement at the junction. In this manner the ratio of power between the two exit ports of the "Tee" coupler can easily be controlled by the relative offset of the junction.

In view of the above findings it is also concluded that additional, detailed investigations of this technique should be made to determine its practical applications. Of particular interest would be to repeat the experimental procedure of this thesis using differential micrometers for the micropositioners and an improved fixture where the end separation and tilt can be eliminated.

REFERENCES

1. Michael K. Barnoski, Fundamentals of Optical Fiber Communications, (New York, Academic Press, Inc., 1976), p. ix.

2. Donald C. O'Shea, W. Russell Callen, and William T. Rhodes, Introduction to Lasers and Their Applications, (Reading, Mass., Addison-Wesley Publishing Co., 1977), p. 6.

3. C. P. Sandbank, "Fiber Optic Communications: A Survey," Electrical Communication, vol. 50, no. 1, (1975), p. 20.

4. D. Gloge, "Offset and Tilt Loss in Optical Fiber Splices," Bell System Technical Journal, vol. 55, no. 7, (September 1976), p. 905.

5. David Halliday and Robert Resnick, Physics, (New York, John Wiley and Sons, 1967), pp. 1013-1016.

6. Ibid., p. 1013.

7. Ibid., p. 1024.

8. N. S. Kapany, Fiber Optics, (New York, Academic Press, Inc., 1967), pp. 7-9.

9. Halliday and Resnick, p. 1024.

10. Kapany, pp. 7-9.

11. Ibid.

12. Barnoski, p. 2.

13. Kapany, pp. 12 & 26.

14. Sandbank, p. 21.

15. Kapany, p. 12.

16. Ibid., p. 26.

17. M. M. Ramsay, G. A. Hockham, and K. C. Kao, "Propagation in Optical Fiber Waveguides," Electrical Communication, vol. 50, no. 3, (1975), pp. 162-163.

18. Steward E. Miller, Enrique A. J. Marcatili, and Tingye Li, "Research Toward Optical-Fiber Transmission Systems," Proceedings of the IEEE, vol. 61, no. 12, (December 1973), pp. 1704-1706.

19. Ibid.

20. Tom Ormond, "Fiber-Optic Components --- Today's Devices Make System Designs More Attractive," EDN, vol. 23, no. 9, (May 1978), pp. 48-53.

21. Sandbank, p. 21.

22. D. Gloge and E. A. J. Marcatili, "Multimode Theory of Graded-Core Fibers," Bell Systems Technical Journal, vol. 52, no. 9, (November 1973), p. 1569.

23. Ibid., p. 1568.

24. C. M. Miller, "Transmission vs. Transverse Offset for Parabolic-Profile Fiber Splices with Unequal Core Diameters," Bell System Technical Journal, vol. 55, no. 7, (September 1976), p. 918.

25. Ramsay, Hockham, and Kao, p. 163.

26. Ibid.

27. Sandbank, p. 20.

28. Barnoski, pp. 27-29.

29. Donald B. Keck, "Transmission Properties of Optical Fiber Waveguides," Proceedings of the Society of Photo-Optical Instrumentation Engineers -- Guided Optical Communications, vol. 63, (August 1973), pp. 4 & 5.

30. Ibid.

31. Barnoski, pp. 28 & 29.

32. Ramsay, Hockham, and Kao, pp. 166 & 167.

33. Ibid.

34. Ibid.

35. D. Gloge, P. W. Smith, D. L. Bisbee, and E. L. Chinnock, "Optical Fiber End Preparation for Low-Loss Splices," Bell System Technical Journal, vol. 52, no. 9, (November 1973), pp. 1579-1588.

36. K. S. Gordon, E. G. Rawson, and R. E. Norton, "Splice Losses in Step Index Fibers: Dependency on Fiber-Break Angle," Applied Optics, vol. 16, no. 9, (September 1977), pp. 2372-2374.

37. Ibid.

38. Barnoski, pp. 94-105.

39. D. L. Bisbee, "Measurement of Loss Due to Offsets and End Separations of Optical Fibers," Bell System Technical Journal, vol. 50, no. 10, (December 1971), pp. 3159-3167.

40. T. C. Chu and A. R. McCormick, "Measurements of Loss Due to Offset, End Separation, and Angular Misalignment in Graded Index Fibers Excited by an Incoherent Source," Bell Systems Technical Journal, vol. 57, no. 3, (March 1978), pp. 595-602.

41. D. Marcuse, "Loss Analysis of Single-Mode Fiber Splices," Bell Systems Technical Journal, vol. 56, no. 5, (May-June 1977), pp. 703-708.

42. Barnoski, pp. 98-105.

43. Chu and McCormick, pp. 595-602.

44. Ibid.

45. Ibid.

46. Ibid.

47. Robert M. Hawk, Frank L. Thiel, "Low Loss Splicing and Connection of Optical Waveguide Cables," Proceedings of the Society of Photo-Optical Instrumentation Engineers --- Guided Optical Communications, vol. 63, (August 1975), p. 112.

48. Ibid.

49. Ibid.

50. Ibid.

51. Gloge, Smith, Bisbee, and Chinnock, pp. 1579-1588.

52. L. Jeunhomme and J. P. Pocholle, "Selective Mode Excitation of Graded Index Optical Fibers," Applied Optics, vol. 17, (1978), pp. 463-467.

53. C. M. Miller, pp. 917-927.

54. C. M. Miller, p. 918.

55. Gloge and Marcatili, p. 120.

56. C. M. Miller, p. 918.

57. Gloge and Marcatili, p. 121.

58. Ibid.

59. C. M. Miller, p. 918.

60. Ibid.

61. C. M. Miller, p. 919.

62. Ibid.

63. Ibid.

64. Kapany, p. 26.

65. Jeunhomme and Pocholle, p. 465.

66. K. Ogawa, "Simplified Theory of the Multimode Fiber Coupler," Bell System Technical Journal, vol. 56, no. 5, (May-June 1977), pp. 729-745.

67. Peter D. McIntyre and Allan W. Snyder, "Power Transfer Between Optical Fibers," Journal of the Optical Society of America, vol. 63, no. 12, pp. 1518-1527.

68. A. H. Cherin and E. J. Murphy, "Quasi-Ray Analysis of Crosstalk Between Multimode Optical Fibers," Bell System Technical Journal, vol. 54, no. 1, (January 1975), pp. 18-44.

69. Cherin and Murphy, pp. 22-24.

70. Ibid.

71. Ibid.

72. Cherin and Murphy, p. 25.

73. Ibid., pp. 25-27.

74. Gloge, Smith, Bisbee, and Chinnock, p. 1586.

75. Ibid., p. 1587.

76. Gordon, Rawson, and Norton, p. 2373.

77. Bisbee, p. 3160.